Journal of Hazardous Materials 406 (2021) 124615

Contents lists available at ScienceDirect

Journal of Hazardous Materials

journal homepage: www.elsevier.com/locate/jhazmat

Reduction of iron (hydr)oxide-bound arsenate: Evidence from high depth resolution sampling of a reducing aquifer in Yinchuan Plain, China

Yuqin Sun [a,b,c], Jing Sun [d], Athena A. Nghiem [e], Benjamin C. Bostick [b,e], Tyler Ellis [e], Long Han [b,c], Zengyi Li [b,c], Songlin Liu [b,c], Shuangbao Han [b,c], Miao Zhang [b,c], Yu Xia [b,c], Yan Zheng [b,c,*,1]

[a] College of Engineering, Peking University, Beijing 100871, China
[b] State Environmental Protection Key Laboratory of Integrated Surface Water-Groundwater Pollution Control, School of Environmental Science and Engineering, Southern University of Science and Technology, Shenzhen 518055, China
[c] Guangdong Provincial Key Laboratory of Soil and Groundwater Pollution Control, School of Environmental Science and Engineering, Southern University of Science and Technology, Shenzhen 518055, China
[d] State Key Laboratory of Environmental Geochemistry, Institute of Geochemistry, Chinese Academy of Sciences, Guiyang, China
[e] Lamont-Doherty Earth Observatory, Columbia University, 61 Route 9W, Palisades, NY 10964, United States

ARTICLE INFO

Keywords:
Groundwater
Arsenic
Iron mineralogy
X-ray absorption near edge structure (XANES)
X-ray absorption fine structure (EXAFS)

ABSTRACT

Sediment in fluvial-deltaic plains with high-As groundwater is heterogenous but its characterization of As and Fe oxidation states lacks resolution, and is rarely attempted for aqueous and solid phases simultaneously. Here, we pair high-resolution (> 1 sample/meter) Fe extended fine-structure spectroscopy (EXAFS, n = 40) and As X-ray absorption near-edge spectroscopy (XANES, n = 49) with groundwater composition and metagenomics measurements for two sediment cores and their associated wells (n = 8) from the Yinchuan Plain in northwest China. At shallower depths, nitrate and Mn/Fe reducing sediment zones are fine textured, contain 9.6 ± 5.6 mg kg^{-1} of As(V) and 2.3 ± 2.7 mg kg^{-1} of As(III) with 9.1 ± 8.1 g kg^{-1} of Fe(III) (hydr)oxides, with bacterial genera capable of As and Fe reduction identified. In four deeper 10-m sections, sulfate-reducing sediments are coarser and contain 2.6 ± 1.3 mg kg^{-1} of As(V) and 1.1 ± 1.0 mg kg^{-1} of As(III) with 3.2 ± 2.6 g kg^{-1} of Fe(III) (hydr) oxides, even though groundwater As concentrations can exceed 200 μg/L, mostly as As(III). Super-enrichment of sediment As (42–133 mg kg^{-1}, n = 7) at shallower depth is due to redox trapping during past groundwater discharge. Active As and Fe reduction is supported by the contrast between the As(III)-dominated groundwater and the As(V)-dominated sediment, and by the decreasing sediment As(V) and Fe(III) (hydr)oxides concentrations with depth.

1. Introduction

Elevated levels of geogenic arsenic (As) in groundwater used for drinking water supply have been detected in over 70 countries, causing the exposure to As from groundwater to be a major threat to public health (Smedley and Kinniburgh, 2002). A recent machine-learning based geostatistical model has estimated that 94–220 million people are at risk of exposing to unsafe level of As in groundwater that is above the World Health Organization's provisional guideline value of 10 μg/L for drinking water, with 94% of the affected being in Asia (Podgorski and Berg, 2020). Because As also contributes significantly to soil-derived health risks (Antoniadis et al., 2019), understanding the coupling among biogeochemical cycles of As, Fe (O'Day et al., 2004a) and S (Bostick et al., 2004; Du Laing et al., 2009; O'Day et al., 2004a) in bio-hydro-lithospheres is crucial (Hussain et al., 2021; Kumarathilaka et al., 2018), and the need to mitigate the health risks has led to research on low cost and environmental friendly treatments (Shakoor et al., 2019; Amen et al., 2020). Especially relevant is the sediment iron (Fe) mineralogy due to the high affinity of As for the surface of Fe(III) (hydr) oxides (Bowell, 1994). Further, reductive dissolution and transformation of As-bearing Fe(III) (hydr)oxides is widely accepted as the key mechanism behind the As-tainted groundwater in reducing aquifers

* Correspondence to: Southern University of Science and Technology, Shenzhen, Guangdong 518055, China.
E-mail address: yan.zheng@sustech.edu.cn (Y. Zheng).
[1] ORCID 0000-0001-5256-9395.

https://doi.org/10.1016/j.jhazmat.2020.124615
Received 1 September 2020; Received in revised form 28 October 2020; Accepted 16 November 2020
Available online 18 November 2020

(e.g. Fendorf et al., 2010; Harvey et al., 2002; Natasha et al., 2021; Wallis et al., 2020; Smedley et al., 2005). Yet this prevailing paradigm is established mostly on the basis of aqueous geochemical characterization of the As-rich groundwater (Zheng et al., 2004), correlations between bulk and sequentially-extracted As and Fe concentrations in sediment depth profiles (Berg et al., 2001), or from *ex situ* incubation (Van Geen et al., 2004). Despite intense research on the groundwater As issues (e.g. Harvey et al., 2002; Frohne et al., 2011; LeMonte et al., 2017), the direct evidence for that reduction of sediment As associated with Fe(III) (hydr) oxides causes elevated As concentration in groundwater remains rare, especially lacking is the paired speciation analysis of As and Fe in aqueous and solid phases to support the active reduction of both As and Fe.

To understand the current and future distribution of groundwater As, it is critical to identify the minerals hosting and releasing As in aquifers and their redox transformations. Despite this realization, sediment Fe mineralogy is seldom investigated relative to more abundant studies of groundwater aqueous chemistry (Fendorf et al., 2010; Zheng et al., 2005). One of the reasons is that high-As groundwater occurs frequently in fluvial-deltaic aquifers where sediment deposits are notoriously heterogenous (Smedley and Kinniburgh, 2002; Goodbred and Kuehl, 2000; Anderson et al., 1999), contributing to a large degree of spatially heterogenous groundwater As distributions from local to basin scales (Berg et al., 2001; van Geen et al., 2003; Yang et al., 2015). In addition, quantifying Fe mineral composition in heterogenous and complex sediments and soils is analytically challenging (Postma et al., 2010; Sun et al., 2018). To date, most evidences supporting that As-bearing sediment Fe(III) (hydr)oxides is the culprit for high-As groundwater are based on sequential extraction, such as the Bengal Basin (Nickson et al., 2000; Reza et al., 2010b), the Mekong delta (Kocar et al., 2008; Kocar and Fendorf, 2009), the Red River delta (Berg et al., 2001), the Hetao Plain (Qiao et al., 2020; Shen et al., 2018) and the Datong Basin (Xie et al., 2008) in the Yellow River corridor like the Yinchuan Plain in this study. However, interpreting these extraction data is not only ambiguous but also limited by its capability of delineating speciation. Anaerobic phosphate extraction has been used to evaluate sediment As speciation in Bangladesh, with only 2 of 4 samples showing consistent As (III)% with XANES data (Jung et al., 2012). A bigger problem is iron because even the hot-HCl extracted Fe(II)/Fe ratio used to evaluate redox condition (Horneman et al., 2004), is only a portion of the bulk Fe (Aziz et al., 2017).

Among many mineralogical techniques, synchrotron X-ray absorption spectroscopy, especially EXAFS, has proven to be advantageous in quantifying Fe mineralogy in sediments and soils through linear combinations of reference spectra or theoretical shell fitting (O'Day et al., 2004b; Sun et al., 2018). To date, only a handful of studies have characterized Fe mineralogy in geogenic high-As aquifers using EXAFS, with far less sediment Fe and As mineralogy data than bulk Fe and As concentrations (Table S1) (Aziz et al., 2017; Schaefer et al., 2017; Quicksall et al., 2008; Stuckey et al., 2015; Gnanaprakasam et al., 2017). For example, only 8 samples from one 30-m core in the Jianghan Plain were included for As XANES (n = 9) and Fe EXAFS (n = 8) analyses while the sampling resolution for bulk chemistry was roughly one sample per 1.5 m (Schaefer et al., 2017). High-resolution sampling of both sediment and water offers a unique opportunity to study redox transformations across chemical gradients that are otherwise difficult to characterize, and in doing so, help to develop an unambiguous understanding of which phases host As, and which are sources of groundwater As in reducing aquifers, and the relative roles of Fe and As reduction in the formation of groundwater As.

The main objectives of this study were therefore (i) to characterize sediment Fe and As mineralogy in As-rich reducing aquifers at high depth resolution, (ii) to delineate the carrier phases of As and the transformations of those phases that affect As release into groundwater, and (iii) to identify geogenic processes that result in the enrichment of As in heterogeneous sediments. This research focuses on two sediment cores, YCA and YCB, from the Yinchuan Plain, with semi-confined Quaternary aquifers consisting of late Pleistocene and Holocene unconsolidated alluvial-lacustrine sediments. It has been shown that shallow (< 40 m) groundwater in the Yinchuan Plain has As concentration between 3 and 177 μg/L (n = 142) (Han et al., 2013). Both cores were sampled at high-spatial resolution (each m or higher, to 30 m for YCA and to 40 m for YCB) to determine As speciation via XANES and Fe mineralogy using EXAFS. Additional measurements on the sediments included chemical extraction and X-ray Fluorescence (XRF). The redox zonation of the aquifer was described using mineralogical data in combination with changes in groundwater composition and sedimentology as a function of depth. In addition, metagenomic analysis of microbial community was conducted within the Fe/Mn-reducing zones to identify specific microbial processes affecting the redox chemistry of As and Fe. These data provide a window into the processes that control groundwater As levels through both the release and accumulation of As in sediments.

2. Methods

2.1. Hydrogeologic setting

The study area is located in the northern Yinchuan Plain, northwestern China (Fig. 1), where a high subsidence rate of 0.22 cm per year has resulted in substantial accumulation of Quaternary sediments up to 2000 m thick (Han et al., 2013; Wang et al., 2015). The northern plain consists of multiple layers of alluvial and lacustrine deposits forming an unconfined shallow aquifer with depths between 10 and 40 m and two confined aquifers with depths between 25 and 60 m and > 140 m (Han et al., 2013). The groundwater table fluctuates between 0.1 and 5 m below ground level (mbgl) for the unconfined aquifer, partly due to irrigation using water diverted from the Yellow River or the Sand Lake (Fig. 1). The confined aquifer is recharged by lateral flow from the Helan Mountain and infiltration from the unconfined aquifer above (Han et al., 2013).

The study sites (YCA: 38°49'48.20'' N, 106°21'14.04'' E; YCB: 38°50'41.53'' N, 116°22'24.57'' E) are located within a strip of high groundwater As wells between the Helan Mountain and the Yellow River adjacent to the Sand Lake (Fig. 1). About 16% of wells (n = 355) from < 40 m of the Yinchuan Plain contains > 10 μg/L As (Table S2), with the wells containing elevated levels of As forming a distinct belt-like pattern. The two line-like features where high As wells are frequently found in northern Yinchuan Plain reflect presumably paleochannel deposits of the Yellow River formed as the river meandered (Han et al., 2013). Located 2.5 km apart, the YCA site, immediately adjacent to the Sand Lake, has rice fields irrigated by diverted Yellow River water; the YCB site is located in a corn field next to a farmer's house and is irrigated by groundwater containing variable As (100–700 μg/L) drawn from a depth of 60 m.

2.2. Groundwater sampling and chemical analysis

Groundwater samples (n = 8) were obtained in September 2017 in multi-level monitoring wells (MLMWs) installed at the YCA and YCB sites by the China Geology Survey in 2012. Each MLMW consists of seven PVC pipes to reach the desired depth with a screen interval of 15 cm. The 7 depths of MLMWs at YCA are 3, 10, 23, 30, 40, 50 and 60 mbgl; they are 10, 20, 29, 39, 50 and 60 mbgl at YCB. The groundwater samples were collected in the 3, 10, 23 and 30 m depths of YCA; 10, 20, 29 and 39 m depths at YCB. A peristaltic pump (Solinst Model 410) was used to flush each depth for > 20 min until temperature (T), electrical conductivity (EC), pH and oxidation–reduction potential (ORP) monitored by a multiprobe (Thermo, 520M-01A) in a flow cell reached stable values. All samples were filtered (0.22 μm syringe filter, Nylon, Jinteng China) immediately and collected into two 30-mL precleaned HDPE bottles, with an aliquot filtered additionally through an

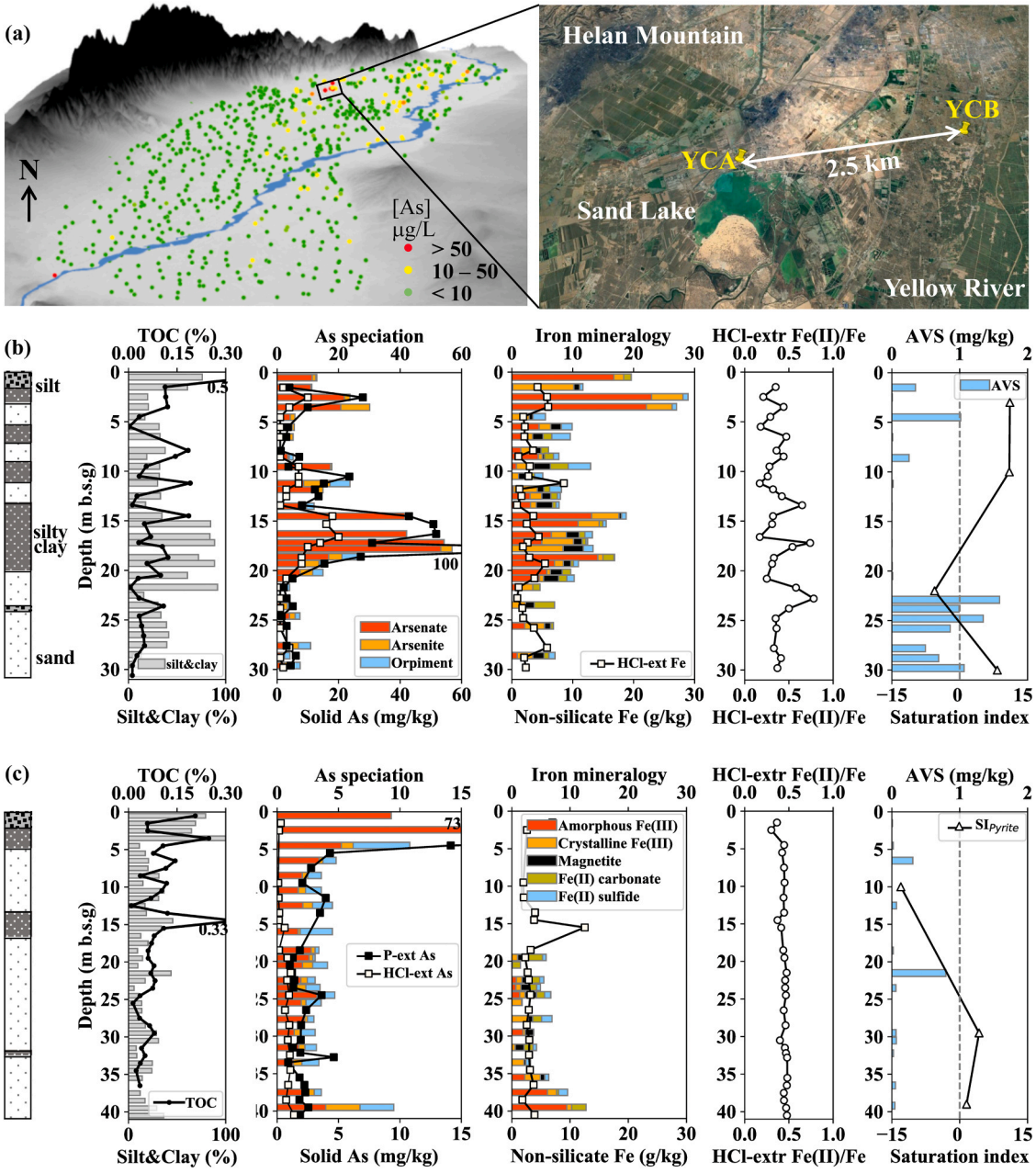

Fig. 1. (a) Location of YCA and YCB sites from the north Yinchuan plain within a belt of high As groundwater wells (left, [As] ranging 0–177 μg/L in 579 wells, 13% wells with [As] > 10 μg/L) between the Helan Mountain and the Yellow River (revised from Han et al. (2013)), with a Google Earth image (right) showing the Sand Lake, irrigation canals, agricultural fields and villages. Lithology sketches, depth profiles of sediment organic carbon content and % silt and clay, sediment bulk (stacked bar), phosphate-extractable and HCl-extractable As concentrations, as well as arsenic speciation determined by XANES; sediment bulk (stacked bar) and HCl-extractable Fe concentrations, as well as iron mineralogy obtained by EXAFS (Fe-silicates were excluded when calculating %iron mineral compositions); HCl-extracted sediment Fe(II)/Fe ratio, concentrations of acid volatile sulfide (AVS) and saturation index of pyrite calculated by PHREEQC (Table S3) using aqueous chemical compositions at YCA (b) and YCB (c).

arsenic speciation cartridge (MetalSoft Center Highland Park, NJ) that retained As(V) to allow for aqueous As(III) analysis (Meng et al., 2001). Samples for dissolved organic carbon (DOC) analysis were filtered with 0.7 μm GF/F filters (Whatman) into 22-mL pre-combusted brown glass bottles. They were preserved at 4 °C before analyzing on Shimadzu TOC-L. Alkalinity was determined by Gran titration in the field. Concentration of H_2S was measured using HACH Method 8131 with a portable spectrophotometer (DR1900, HACH).

Concentrations of anions including F^-, Cl^-, SO_4^{2-} and NO_3^- were measured by ion chromatography (ICS-90, DIONEX) at the Institute of Geochemistry, Chinese Academy of Sciences, following the standard protocol of EPA method 300. Concentrations of dissolved As, Fe, P, S, Ca, Mg, K, Na were measured by high resolution inductively coupled plasma mass spectrometry (ICPMS) following a method with a detection limit for As of < 1 μg/L (Cheng et al., 2004) at Lamont–Doherty Earth Observatory. Standard reference materials (NIST1640a and NIST1643e) were used for quality assurance and control. Four tested NIST1643e samples with 60.45 μg/L of As and four tested NIST1640a with 8.01 μg/L of As averaged 58.6 ± 0.3 μg/L and 8.0 ± 0.2 μg/L, respectively, with a precision relative standard deviation (RSD) < 4%. Charge balances of cations and anions for all samples were < 10%.

To investigate mineral precipitation and dissolution reactions,

calculation was made using PHREEQC with wateq4f database (Phreeqc Interactive 3.6.2, USGS) for aqueous chemical equilibrium speciation. The aqueous Fe(II)/Fe ratio and saturation index (SI) values of minerals that likely be reacting in the aqueous system were listed with the water chemistry parameters of 7 groundwater samples in Table S3.

2.3. Sediment collection and field analysis

Continuous sediment cores were obtained by a split spoon sampler to a depth of 30 m at YCA in September 2017 and to a depth of 40 m at YCB in April 2018. The sediment cores were sampled immediately in triplicate by inserting three small plastic core sleeves (Φ:25 mm, length: 180 mm) into the center of the larger core inside the split spoon sampler before it was split open, then sealed with end caps. A total of 34 samples from YCA and 42 samples from YCB core were collected for every meter of sediment cored, and in case of lithological changes, additional samples were taken. Care was taken to minimize oxidation. All sediment samples were stored in Mylar bags with O_2 adsorbent, flushed with N_2 gas before sealing. The sediment samples were shipped at ambient temperature within 1 day of collection and stored at 4 °C for chemical analysis or − 80 °C for microbiome assay. Aliquots of sediment samples for synchrotron analysis were collected from the first of the triplicate 18 cm-tubes and placed into 2-mL centrifuge tubes. These samples were preserved in glycerol immediately in the field, and stored anaerobically on ice to the lab and stored at − 20 °C before analysis.

In the evening on the same day of sediment coring, leachable Fe concentrations were measured for additional sediment samples collected from the first (No.1) of 18 cm-cores. These sediment samples were leached with 10 mL of 1.2 M HCl at 80 °C for 30 min in 15 mL centrifuge, followed by Fe(II)/Fe ratio quantified by a colorimetric method using ferrozine (Horneman et al., 2004). The HCl leachate was filtered and saved for analysis.

2.4. Sediment chemical analysis

The second (No.2) of the triplicate 18 cm-cores was removed from anaerobic storage and subsampled for phosphate extraction and acid volatile sulfide (AVS) extraction within one month after coring. Concentration of H_2S from AVS extraction was determined using a portable spectrophotometer (DR1900, HACH) with a methylene blue method. Approximately 10 g of sediment was added in 100 mL MQ water and purged with N_2 gas for 10 min to generate H_2S in a holding flask with 10 mL mixed diamine reagent (Allen et al., 1993). The mixed diamine reagent was mixed by 8.5 mM phenylenediamine and 0.1 M ferric chloride hexahydrate (Allen et al., 1993). Another aliquot of 1 g of sediment was leached by 1 M $Na_2H_2PO_4$ with 0.1 M L-ascorbic at pH 5 (Jung and Zheng, 2006). The sediment samples were added into serum bottles containing extraction solution under N_2 condition and were crimped before shaken for 24 h. Leached solutions from phosphate extraction were collected with a syringe from the crimped serum bottles and filtered through 0.22 μm filter. HCl and phosphate leached solutions were analyzed by HR ICP-MS to quantify the Fe, Mn, S, P and As concentrations similarly as groundwater samples.

Stored sediments were subsampled and homogenized in June 2019 from the third tube (No.3) of the triplicate 18-cm cores. An aliquot was disaggregated and sequentially extracted by 10% H_2O_2 and 10% HCl to remove organic matter and carbonates, and dispersed with 0.05 M $(NaPO_3)_6$ solution for grain-size distribution using a Malvern Mastersizer 2000 laser particle-size analyzer, following a modified version of previous procedure with a precision of ± 1% (Radloff et al., 2017; Hao et al., 2012). For bulk chemistry and organic carbon, another aliquot from the No.3 18-cm tubes was freeze-dried and homogenized. Concentrations of As, Fe and major elements Si, Al etc were determined by X-ray fluorescence spectroscopy (XRF, Tiger S8). Three soil standard reference materials (GSD32, GSS18 and GSS34) were used with reproducibility being < 3% for As, < 0.6% for Fe, < 0.5% for Si and Al. The total organic carbon (TOC) concentration was determined on a TOC Analyzer (multi N/C 3100, Analytic Jena) following removal of carbonate using 1 M HCl (Schumacher, 2002).

2.5. Mineralogy analysis by X-ray absorption spectroscopy

Iron extended X-ray absorption fine structure (EXAFS) spectra and arsenic X-ray absorption near edge structure (XANES) were collected on 49 sediments samples at the Stanford Synchrotron Radiation Laboratory (SSRL) on beamline 4–1 equipped with a Si (220) monochromator ($\varphi = 90°$). For Fe EXAFS, the calibration was carried out with Fe foil at 7112.0 eV. Fe EXAFS spectra were collected in fluorescence mode with a 3 μx Mn filter using a passivated implanted planar silicon (PIPS) detector. For As XANES, the calibration was carried out with Au foil at 11,919 eV. As XANES spectra were collected in fluorescence mode with a Ge filter using a 30-element Ge detector.

Least-squares linear combination fitting (LCF) was applied to quantify the mineralogy fractions in each EXAFS spectrum and XANES spectrum by using SIXpack (Webb, 2005) with previously collected Fe and As mineral references based on published studies on the Holocene aquifers (Sun et al., 2016, 2018; Jung et al., 2012; Kumar et al., 2020). Additionally, principal components analysis (PCA) and target transform analysis were performed to evaluate whether the references selected were suitable and were found to be statistically sound (Figs. S1 and S2).

2.6. Microbiome analysis

Small sediment samples from the first (No.1) tube of YCA cores were used to extract DNA using FastDNA® SPIN Kit for Soil (MP Biomedicals, USA) according to manufacturer's protocol. DNA concentration and purity were determined by NanoDrop One instrument (Thermo Fisher Scientific, Wilmington, DE, USA). Due to the low biomass content in the sediment, only two sediment samples (YCA-1.5 m andYCA-11.2 m) contained enough extracted DNA for metagenomic sequencing. The shotgun metagenomic libraries from the two samples were sequenced on an Illumina Hiseq X-ten platform with 150 bp paired-end strategies at Guangdong MAGIGENE Biotechnology Co., Ltd (Guangzhou, China).

The generated raw sequences were trimmed and quality-filtered using Trimmomatic (Bolger et al., 2014). The qualified sequences were then *de novo* assembled using CLC workbench (Qiagen, Germany), and only contigs longer than 1 kb were reserved for subsequent analysis. After that, a total of 390,476 contigs with an average length of 2423.42 bp from 2 metagenomic samples were obtained. The open reading frames (ORFs) of the contigs were predicted using Prodigal v2.6.3 with a meta model (Hyatt et al., 2010). The relative abundance of each contig was calculated by mapping clean reads to the contigs using bbmap (https://sourceforge.net/projects/bbmap/) with parameters based on previous analysis (Dang et al., 2020) and then normalized by the total number of clean reads. The functional analysis was performed by using PROKKA (Seemann, 2014). The KEGG functional categories were assigned based on PROKKA annotation using a self-written script, and the iron reduction pathway was revealed by FeGenie (Garber et al., 2020). The contigs encoding iron, arsenic or sulfate reduction genes were then assigned into taxonomy using the Kraken (Wood and Salzberg, 2014).

3. Results

3.1. Contrasting groundwater and sediment arsenic speciation in a reducing aquifer

3.1.1. Groundwater and sediment redox condition

The depth profiles of redox-sensitive parameters suggest sequential reduction of NO_3^-, followed by overlapping Mn and Fe reduction and finally SO_4^{2-} (Fig. 2), with sulfate reducing conditions dominating at > 20 m depth at YCA and YCB (Fig. 1). All groundwater are likely anoxic

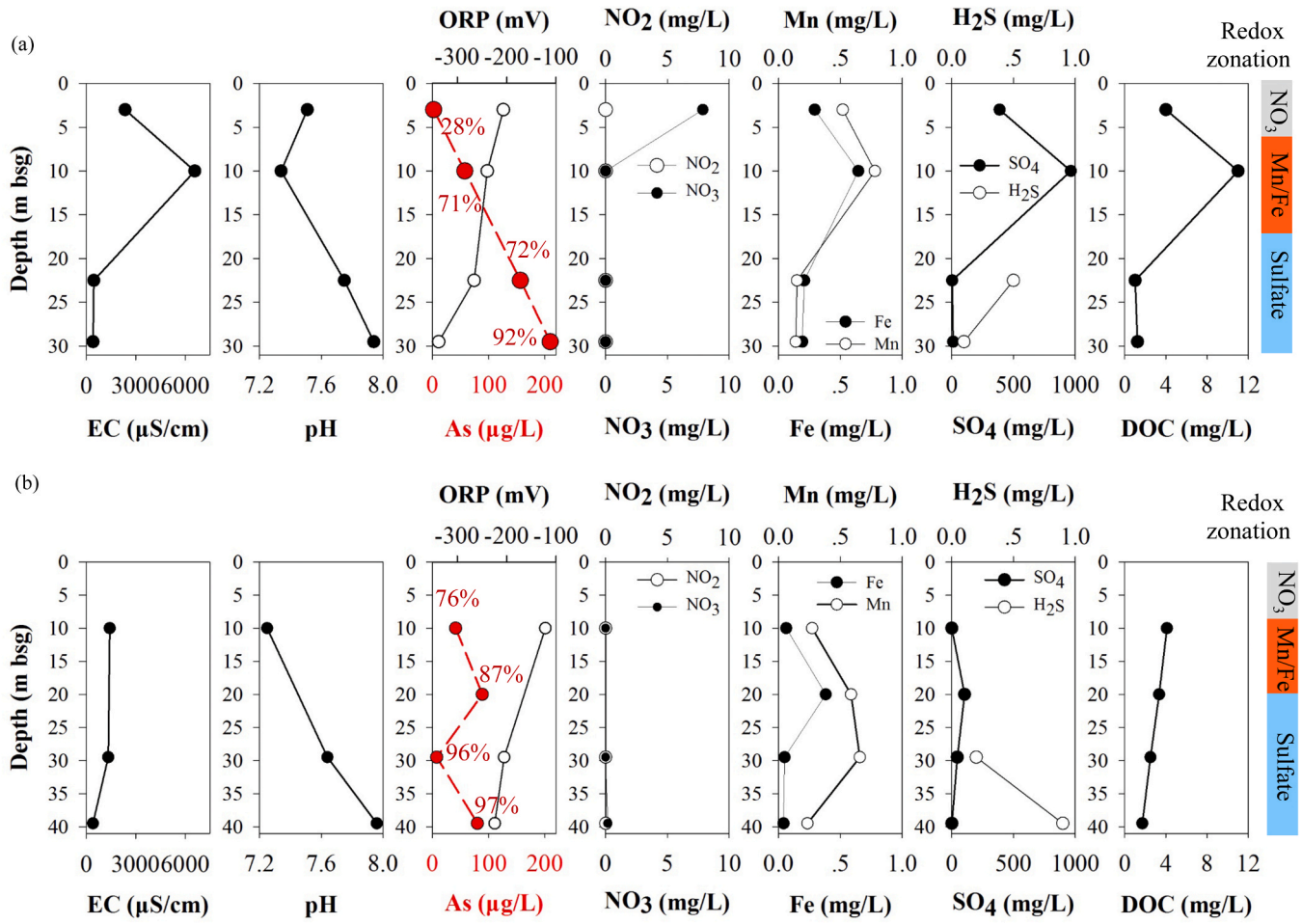

Fig. 2. Depth profiles of field parameters (electrical conductivity, EC; pH; ORP) and lab measurements including total As concentrations with %As as As(III) marked next to the well depth, concentrations of nitrate, nitrite, iron, manganese, sulfate and sulfide, and dissolved organic carbon (DOC) at YCA (a) and YCB (b). Redox zonation is indicated by the colored bar to the right.

as indicated by low DO (Table S3) with non-detectable nitrate (<0.01 mg L^{-1}), except the shallowest well YCA-3 m with 7.8 mg L^{-1} NO_3^-. Groundwater from YCA-3 m is also the least reducing and is undergoing active nitrate reduction, consistent with the lowest %As(III) (28%) found, in contrast with the rest of the 7 wells all with > 70% As (III) (Fig. 2). The depth profiles of groundwater Mn and Fe are similar with each other at both sites, increasing with depth to reach the highest concentrations at mid-depth intervals (YCA-10 m and YCB-20 m & 30 m) then dropping to distinctly lower Fe levels of about 0.2 mg L^{-1} in YCA and 0.05 mg L^{-1} in YCB, respectively (Fig. 2), where the groundwater has entered the sulfate reduction zone. Concentrations of SO_4^{2-} are the highest also at YCA-10 m (950 mg L^{-1}) and YCB-20 m (108 mg L^{-1}), then decrease to 13 mg/L and 2 mg/L in the deepest samples at YCA and YCB, respectively (Fig. 2). Additionally, presence of dissolved sulfide (0.1–0.9 mg L^{-1}) at depths of 22 m & 30 m of YCA and 30 m & 39 m of YCB (Table S3) also supports that the lower half of the sediment columns at both sites are under sulfate reducing conditions. Finally, supersaturation (SI>1) with respective to pyrite at depths of 3 m, 10 m and 30 m of YCA and 29 m and 39 m of YCB is observed, though orpiment first appears at 8.5 m at YCA and 2.5 m at YCB according to XANES (Table S4). The pockets of sulfate reduction at YCA-3 m reflect not only the highly heterogeneous nature of the sediment at 1–10 cm depth scale but also a large supply of dissolved sulfate from irrigation water diverted from the Yellow River (NO_3^-: 11.1 mg L^{-1}, SO_4^{2-}: 8100 mg L^{-1}, Table S3). Nearby the Sand Lake water is brackish (TDS: 3353 mg L^{-1}) with 6.9 mg L^{-1} of NO_3^- and 721 mg L^{-1} of SO_4^{2-} (Table S3). Sediment HCl-extracted Fe(II)/Fe ratio is fairly consistent with depth and averages 0.37 ± 0.14 for YCA and 0.45 ± 0.03 for YCB, respectively (Fig. 1). This ratio is consistent with reducing conditions being prevalent throughout the entire sediment column (Jung et al., 2012; Horneman et al., 2004), as well as that 100% of groundwater Fe is Fe(II) as estimated by aqueous equilibrium in PHREEQC (n = 7, Table S3). AVS is also found at YCA (23–30 m), further supporting the prevalence of sulfate-reducing conditions in the lower half of the sediment column.

3.1.2. *Arsenate in reducing sediment with arsenite in reducing groundwater*

The As K-edge XANES of all sediment samples display a distinct peak of As(V) (Fig. 3). Taking advantage of high depth resolution of at least 1 sample per 1-m interval of sediment analysis (the samples analyzed are aliquots of a homogenized 18-cm section, and transferred into 1 mL centrifugal tube in the field), the data are grouped to 10-m depth interval and categorized as either Fe/Mn-reducing and sulfate-reducing sediments, considering groundwater redox zonation (Fig. 2) as well as the proportion of orpiment determined by XANES (Tables 1 and 2). In the three 10-m sections of Fe/Mn-reducing sediment (YCA 0–20 m and YCB 0–10 m), there is more and highly variable arsenate (19.0 ± 21.3 mg kg^{-1}, 76% ± 19%), less arsenite (1.9 ± 2.5 mg kg^{-1}, 12% ± 11%) and orpiment-As (2.9 ± 8.6 mg kg^{-1}, 11% ± 14%) than those in the four 10-m sections of sulfate reducing sediment (YCA 20–30 m and YCB 10–40 m). The more reducing sediment sections correspond with groundwater sulfate-reducing zones except for YCB10–20 m (Fig. 2). To our surprise, nearly half of the arsenic remains arsenate (2.6 ± 1.3 mg kg^{-1}, 52% ± 17%), with lesser quantities of arsenite (1.1 ± 1.0 mg kg^{-1}, 18% ± 8%) and orpiment-As

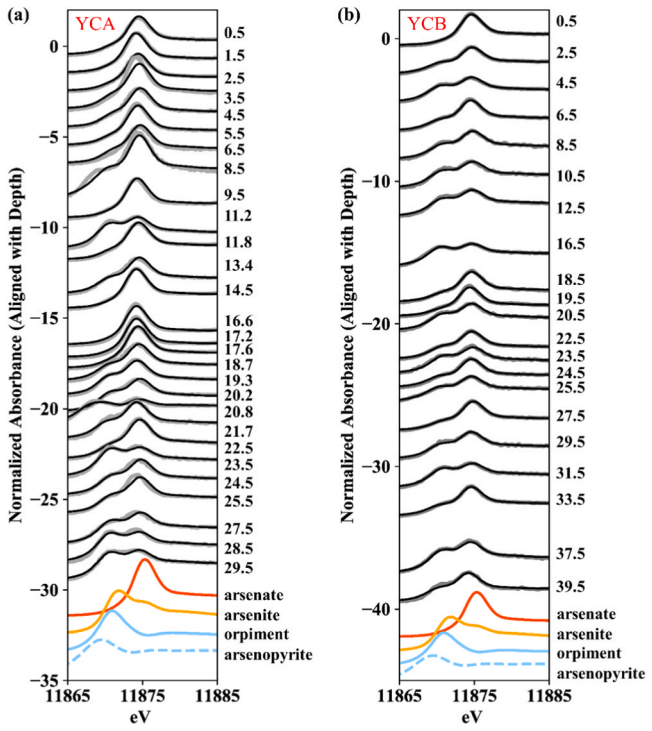

Fig. 3. As XANES spectra (solid gray lines) and fitting curves (solid black lines) for (a) YCA and (b) YCB sediments. The numbers to the right indicate sample depth in meter. The y-axis is shifted according to the depth. Four standards used in linear combination fit are plotted at the bottom.

Table 1
The size fraction, TOC concentration, solid-phase concentrations of As, Fe and their mineralogy in YCA sediments.

Depth range	0–10 m	10–20 m	20–30 m
Silty to sandy ranking	3rd	1st	4th
Thickness of sand (m)	3	2	8.8
Thickness of silt/clay (m)	7	8	1.4
N	10	12	12
Silt & clay (< 63 μm; %)	37 ± 20	58 ± 29 (n = 10)	41 ± 21 (n = 10)
TOC (%)	0.14 ± 0.15	0.08 ± 0.06	0.04 ± 0.03
Bulk As (mg kg^{-1})	12.4 ± 8.4	30.3 ± 15.9	7.2 ± 4.2
P extract As (mg kg^{-1})	7.6 ± 8.1	31.2 ± 24.5	4.6 ± 2.7
HCl extract As (mg kg^{-1})	3.1 ± 3.1	9.6 ± 5.9	1.7 ± 1.1
Bulk Fe (g kg^{-1})	28.7 ± 11.7	30.1 ± 7.7	21.4 ± 7.2
HCl extract Fe (g kg^{-1})	3.3 ± 1.6 (n = 9)	3.3 ± 2.0	3.2 ± 1.6 (n = 9)
HCl ext Fe(II)/Fe ratio	0.34 ± 0.10 (n = 9)	0.38 ± 0.17	0.40 ± 0.10 (n = 9)
N	9	9	10
Arsenate (%)	88 ± 13	77 ± 22	45 ± 16
Arsenite (%)	14 ± 10	14 ± 13	24 ± 6
Orpiment (%)	3 ± 7	9 ± 10	24 ± 14
N	10	11	6
Fe silicates (%)	54 ± 12	60 ± 7	65 ± 4
Ferrihydrite (%)	20 ± 18	18 ± 14	**9 ± 6**
Crystalline Fe(III) (%)	12 ± 9	11 ± 7	**11 ± 7**
Magnetite (%)	4 ± 4	6 ± 4	6 ± 3
Siderite (%)	4 ± 5	3 ± 2	7 ± 5
Mackinawite (%)	6 ± 7	3 ± 2	2 ± 2
AVS (mg kg^{-1})	0.33 ± 0.37 (n = 5)	0.01 ± 0.01 (n = 4)	0.88 ± 0.46 (n = 8)

Notes: Fe-silicates include hornblende, biotite and chlorite identified by EXAFS.

Table 2
The size fraction, TOC concentration, solid-phase concentrations of As, Fe and their mineralogy in YCB sediments.

Depth range	0–10 m	10–20 m	20–30 m	30–40 m
Silty to sandy ranking	2nd	5th	7th	6th
Thickness of sand (m)	5	7	10	9.6
Thickness of silt/clay (m)	5	3	0	0.4
N	10	10	10	12
Silt & clay (< 63 μm; %)	43 ± 31	24 ± 11	18 ± 11	19 ± 9 (n = 10)
TOC (%)	0.04 ± 0.03	0.04 ± 0.02	0.04 ± 0.02	0.02 ± 0.01
Bulk As (mg kg^{-1})	32.7 ± 47.8	4.8 ± 1.7	3.6 ± 0.6	4.5 ± 2.1
P extract As (mg kg^{-1})	19.3 ± 27.4 (n = 5)	2.6 ± 1.1 (n = 4)	2.0 ± 0.8 (n = 7)	2.3 ± 0.9 (n = 9)
HCl extract As (mg kg^{-1})	0.2 ± 0.1 (n = 3)	0.2 ± 0.2 (n = 6)	0.9 ± 0.1 (n = 5)	1.0 ± 0.2 (n = 6)
Bulk Fe (g kg^{-1})	26.0 ± 9.0	19.9 ± 5.7	18.9 ± 1.2	22.5 ± 7.6
HCl extract Fe (g kg^{-1})	3.9 ± 2.2 (n = 3)	5.1 ± 3.8 (n = 6)	3.0 ± 0.5 (n = 5)	3.1 ± 0.7 (n = 6)
HCl-ext Fe(II)/Fe ratio	0.40 ± 0.06 (n = 6)	0.43 ± 0.03 (n = 6)	0.45 ± 0.02 (n = 8)	0.47 ± 0.01 (n = 9)
N	5	5	7	4
Arsenate (%)	69 ± 17	60 ± 19	57 ± 11	51 ± 12
Arsenite (%)	6 ± 5	11 ± 5	13 ± 7	20 ± 6
Orpiment (%)	26 ± 14	29 ± 19	29 ± 7	29 ± 9
N			8	5
Fe silicates (%)			75 ± 11	69 ± 13
Ferrihydrite (%)			**3 ± 4**	**14 ± 13**
Crystalline Fe (III) (%)			**6 ± 4**	**8 ± 5**
Magnetite (%)			6 ± 4	3 ± 3
Siderite (%)			7 ± 6	3 ± 3
Mackinawite (%)			3 ± 3	4 ± 3
AVS (mg kg^{-1})	0.11 ± 0.14 (n = 3)	0.05 ± 0.02 (n = 2)	0.31 ± 0.35 (n = 4)	0.05 ± 0.02 (n = 3)

Fe-silicates include hornblende, biotite and chlorite identified by EXAFS.

(1.4 ± 1.0 mg kg^{-1}, 27% ± 13%) (Tables 1 and 2). High-resolution sampling has also identified super high As zones in both cores, reaching 100 mg kg^{-1} and 133 mg kg^{-1} in YCA-17.6 m and YCB-2.5 m, respectively, much higher than As levels in other intervals and the Upper Crustal abundance of 5.7 mg kg^{-1} (Hu and Gao, 2008). In all, 7 of 43 samples (14.5–17.6 m in YCA, 1.5 and 2.5 m in YCB) contain As significantly above mean values ($p < 0.05$), or 63, 55 and 14 mg kg^{-1} for bulk, phosphate-extracted and HCl extracted As, respectively. Similar zones of enrichment have been observed in shallow Yinchuan Plain sediment (Guo et al., 2014). Excluding these As enriched zones, the average concentrations of bulk, phosphate-extracted and HCl extracted As are 7.9 ± 6.3 mg kg^{-1} (n = 68), 5.8 ± 6.5 mg kg^{-1} (n = 48), and 2.2 ± 2.5 mg kg^{-1} (n = 43) respectively.

Like sediment from YCA and YCB, the proportion of As(III) in groundwater increases with depth as the groundwater becomes progressively more reducing as indicated by more negative ORP values (Fig. 2). At YCA, groundwater [As] increases with depth from 2.1 μg L^{-1} at 3 m to 209 μg L^{-1} at 30 m, accompanied by an increase of %As(III) from 28% to 92% (Fig. 2a). At YCB, groundwater [As] increases from 41.2 μg L^{-1} at 10 m to 79.9 μg L^{-1} at 39 m, although there is a minimum [As] of 7.5 μg L^{-1} at 29 m. Despite this reversal in groundwater [As] at YCB, %As(III) systematically increases from 76% to 97% from 10 m to 39 m like YCA (Fig. 2b). Prior study has found that on average 90% of groundwater As is As(III) for 54 wells with depths between 7 and 250 m (Guo et al., 2014).

3.2. Oxidized iron minerals detected in sulfate-reducing sediment

Iron silicates (63 ± 12%) are the most abundant Fe minerals. These minerals contain both Fe(II) and Fe(III) that are much less reactive than (hydr)oxides. We model these iron silicate minerals through linear combination fits with hornblende, an Fe(II/III) amphibole, biotite, an Fe (II) sheet silicate, and chlorite (an intercalated, large Fe(III) clay mineral). Linear combination fits indicate that much of the Fe is found in these phases, or others with similar structure. Overall linear combination fits of Fe EXAFS of 27 and 13 sediment samples from YCA and YCB, respectively, indicate that sediments on average contain 44 ± 10% hornblende, 18 ± 10% biotite and 1 ± 2% chlorite (Fig. 4, Tables S5 and S6). Fe(III) (hydr)oxides (24 ± 14%) including ferrihydrite (14 ± 14%), goethite (6 ± 8%) and hematite (4 ± 3%), are less abundant but respond more strongly to redox state. Mixed Fe(II)-Fe(III) and secondary Fe(II) minerals constitute small parts of the iron mineral pool (5% ± 4% magnetite, 5% ± 5% siderite and 4% ± 4% mackinawite). The sediments in 3 out of 4 sulfate reducing sections (YCA 20–30 m and YCB 20–40 m) are composed of 70% ± 11% (14.8 ± 5.5 g kg^{-1}) Fe-silicates (Tables 1 and 2), higher than that in 2 out of 3 Fe/Mn-reducing sections (YCA 0–20 m) of 57% ± 10% (15.8 ± 4.1 g kg^{-1}). Similar trends hold in YCB (Figs. 1c and 2b) except for more sulfide-mineral phases associated with the sulfate reducing sections thus are not described.

To allow for a more direct comparison of the Fe(III) (hydr)oxides that participates in active redox cycling, the proportions of amorphous Fe (III) (hydr)oxides represented by ferrihydrite and nanocrystalline goethite (which is fit as ferrihydrite), crystalline Fe(III) (hydr)oxides represented by goethite and hematite, mixed Fe(III)-Fe(II) minerals represented by magnetite, and Fe(II) carbonates (siderite) and sulfides (mackinawite) are calculated for the non-silicate iron fraction for all 40 sediment samples (Fig. 1). Depth profiles show that finer sediments (silt and silty clay from YCA) contain > 10 g kg^{-1} non-silicate Fe with amorphous Fe(III) (hydr)oxides being the most abundant, while the more sandy sediments from both YCA and YCB in general contain < 10 g kg^{-1} non-silicate Fe with more crystalline Fe(III) (hydr)oxides, except for the 2 deepest samples at YCB (39 m and 40 m) where the amorphous Fe(III) (hydr)oxides remain abundant. Further, Fe(III) (hydr) oxides in the Fe/Mn reducing sediment sections (YCA 0–20 m) averaged 30% ± 14% of 9.7 ± 7.4 g kg^{-1} non-silicate iron (Table 1 and Fig. 1). Fe (III) (hydr)oxides, averaging 17% ± 10% of 3.2 ± 2.6 g kg^{-1} non-silicate iron, are detected in sulfate reducing sediments (YCA 20–30 m and YCB 20–40 m, Table 2 and Fig. 1). A comparison of Fe(III) (hydr) oxides concentrations in Fe/Mn reducing sediments and in sulfate reducing sediments is discussed later (Section 4.1).

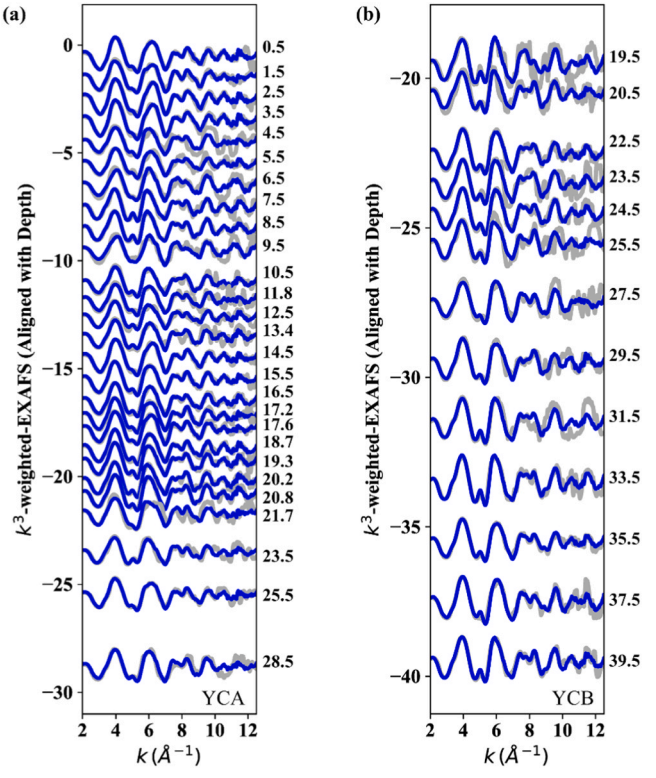

Fig. 4. Fe EXAFS spectra (gray lines) and fitting curves (blue lines) in (a) YCA and (b) YCB sediments with sediment sample depth (unit: meter) marked to the right. (For interpretation of the references to color in this figure legend, the reader is referred to the web version of this article.)

3.3. Enrichment of oxidized arsenic and iron in fine-grained Fe/Mn reducing sediment

Because the Yinchuan sediment contains interbedded sands and fine sediments typical of alluvial-fluvial depositional environment, a sediment core sample of 18 cm length does not fully represent or sample the variability of each entire 1 m interval examined in our high-resolution sectioning. We used a simple approach to reduce sampling bias associated with subsampling sediment cores. For every 10 m depth interval, 10–12 measurements of sediment properties are combined within each 10-m section, with the mean and variance reported (Tables 1 and 2). The thickness of sand or silt/clay layers, along with grain size data, are used to rank the 7 sections in the order of increasing sediment particle size as shown in Fig. 5. The median TOC concentrations for the two silty sections in YCA (0–10 m and 10–20 m) are 0.11% and 0.06%, respectively (Fig. 5f), significantly higher than that of 0.03% for the four sections of more sandy sediments (YCA 20–30 m and YCB 10–40 m) (Mann–Whitney U test, $Z = -2.96$, $p < 0.001$). The median TOC for the finer, silty section of YCB 0–10 m is 0.03%, and is not significantly different with the 4 more sandy sections (Mann–Whitney U test, $Z = -1.72$, $p = 0.085$).

When the seven 10-m sediment core sections are organized based on grain size (Tables 1 and 2), the median concentrations of bulk As decrease as the sediment section becomes more sandy and are in the order of: 25, 9.4, 8.7, 5.0, 4.4, 3.5 and 3.5 mg kg^{-1} (Fig. 5a). When the four sandy sections (YCA 20–30 m and YCB 10–40 m) are combined as a group for comparison with each of the fine-grained sections, and mean concentration of bulk As (5.1 ± 3.0 mg kg^{-1}) is significantly lower than 30.3, 32.7 and 12.4 mg kg^{-1} in YCA 10–20 m, YCB 0–10 m and YCA 0–10 m, respectively ($p = 0.001$). Somewhat less intuitive is that these three finer sediment sections at shallower depths closer to land surface are Fe/Mn reducing according to groundwater redox zonation and % orpiment levels, which are significantly lower than that of the sulfate reducing sediments ($p < 0.001$). Consistent with expectation is that these three 10-m sections of mostly silty, Fe/Mn-reducing sediments all contain significantly higher proportions 76% ± 19% of As as As(V) than that of the four 10-m sections of mostly sandy, sulfate reducing sediments (52% ± 17%) from deeper depths ($p < 0.001$). The median concentrations of bulk Fe of the 7 sections are: 31.7, 25.7, 24.1, 18.9, 18.4, 19.7 and 18.6 g kg^{-1} (Fig. 5d). The median bulk Fe concentration of the four 10-m sandy sediment sections as a group is 18.9 g kg^{-1}, significantly lower than that of 27.0 g kg^{-1} ($p = 0.001$) for the three 10-m silty sections of sediments. The four sandy, more reducing sections at deeper depths also contain significantly lower Fe(III) (hydr)oxides consisted of ferrihydrite and crystalline Fe(III) mineral (16 ± 10%) including hematite and goethite than those of YCA 0–10 m (32 ± 16%, $p = 0.007$) and YCA 10–20 m (29 ± 12%, $p = 0.010$).

Sediment As and Fe concentrations decrease with the silicate (Si) to aluminum (Al) ratio (Fig. 6), with the higher Si/Al ratio suggesting less aluminum-silicate rich clay so a proxy for coarser, more sandy sediments. The 3 sections of finer grained sediments (YCA 0–20 m and YCB 0–10 m) show a large degree of variability in terms of concentrations of bulk As and Fe, as well as the Si/Al ratios, reflecting the heterogeneity in

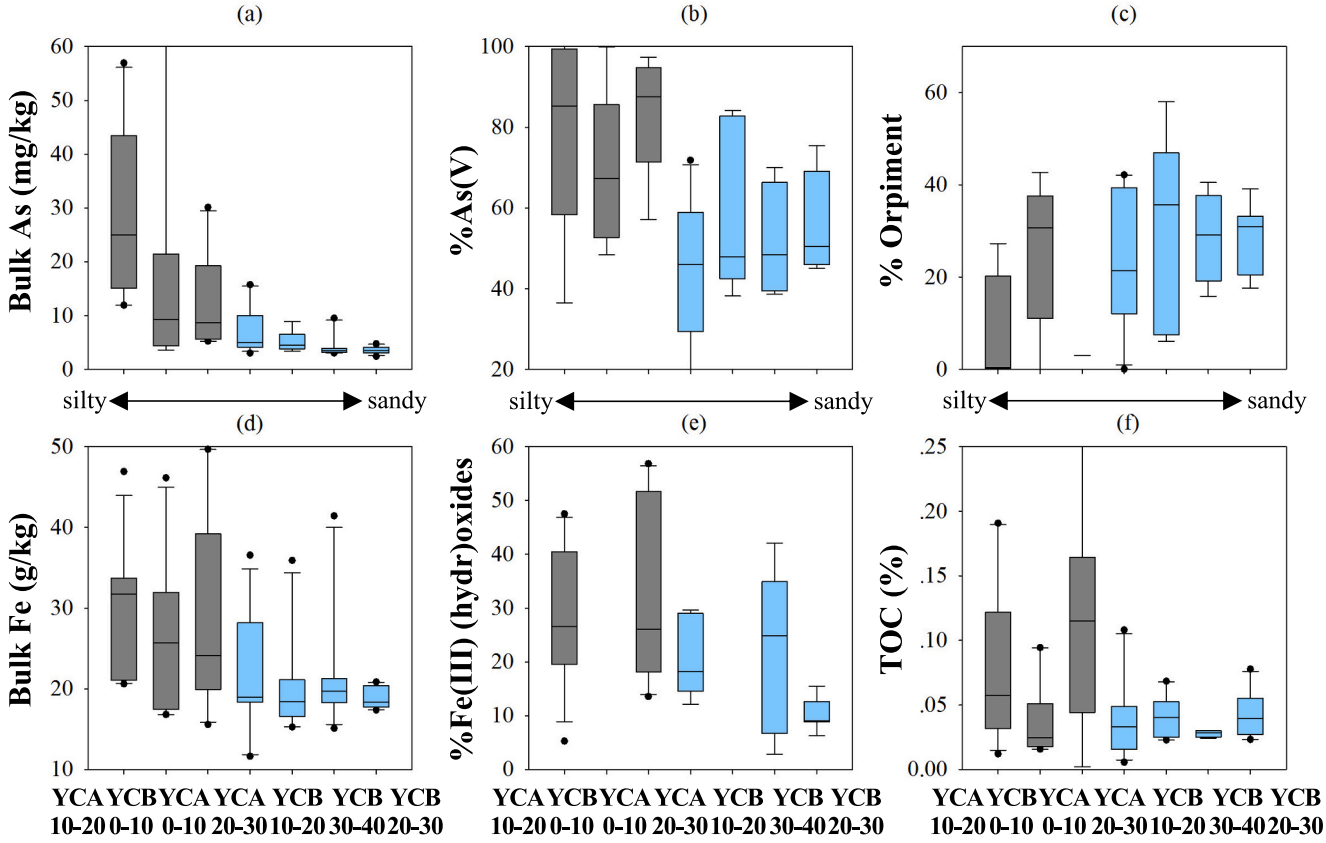

Fig. 5. Box plots for bulk arsenic (a), fraction of AsV (b), fraction of orpiment (c), bulk Fe (d), fraction of FeIII minerals including crystalline and amorphous iron (e) and TOC content (f) in seven 10-m thick sections for YCA and YCB sediments, each sampled at 1 m depth interval with 10 sediment samples, with three sections YCA 10–20 m and 20–30 m and YCB 30–40 m with 2 additional samples.

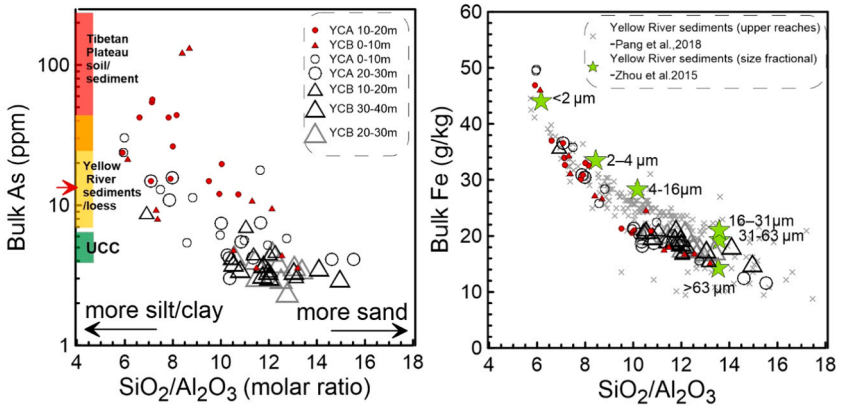

Fig. 6. Comparison of bulk As and Fe concentrations between YCA and YCB sediments samples and the bulk sediments (Pang et al., 2018), size fractional sediments (Zhou et al., 2015) from the upper stretch of the Yellow River. The red arrow to the y-axis represents the median As concentration of yellow river sediments. (For interpretation of the references to color in this figure legend, the reader is referred to the web version of this article.)

such sedimentary deposits.

3.4. Relative abundance of arsenic reducing bacteria in two Fe/Mn-reducing sediments

Microbiome analysis of metagenomic data obtained for two sediments from the fine grained and Fe/Mn reducing sections with above median value TOC concentrations (0.11% in YCA-1.5 m and 0.19% in YCA-11.2 m) has identified dozens of bacterial genera possessing known genes capable of reducing arsenic, with some of these genera (*Pseudomonas*, *Bradyrhizobium*, *Rhizobium*, *Staphylococcus* and *Sulfuricella*) also known to reduce iron (Fig. 7). Only arsenic and iron reducing genera with relative abundance $> 10^{-4}$ are included. Of these genera, several previous isolation organisms studies on *Acinetobacter*, *Psychrobacter* (Liao et al., 2011), *Comamonas* (Yang et al., 2012), *Alishewanella* (Shah and Jha, 2013) and *Staphylococcus* (Ji and Silver, 1992), have confirmed their ability of arsenic reduction. Isolated *Staphylococcus* is also capable of iron reduction (Lascelles and Burke, 1978).

The total abundance of arsenic-reducing genera is 1.33% for YCA-11.2 m, which is higher than that of 0.20% for YCA-1.5 m, but the diversity of arsenic-reducing community is higher in YCA-1.5 m (Fig. 7). Among all the arsenic reducing genera identified, *Acinetobacter*,

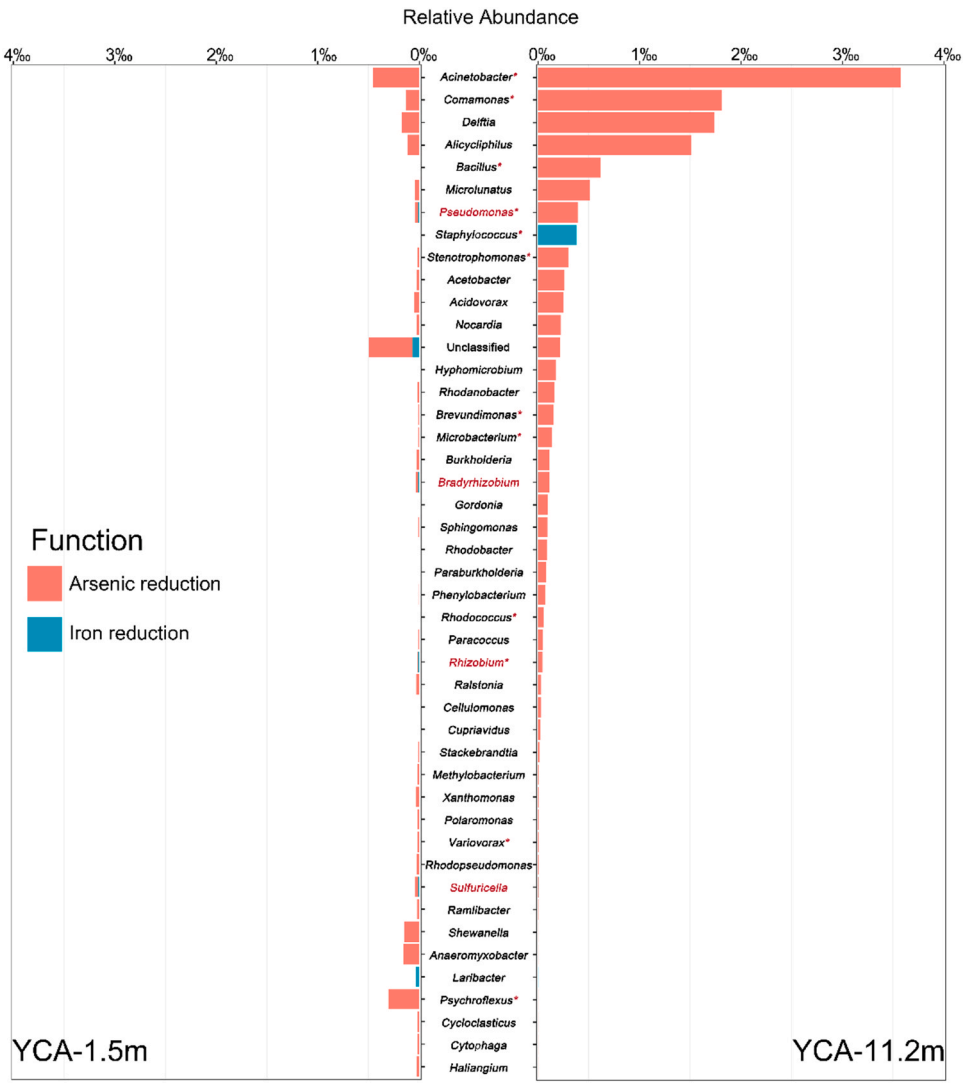

Fig. 7. Relative abundances of 45 arsenic-reducing and 6 iron-reducing genera in YCA-1.5 m and YCA-11.2 m metagenome. A genus is identified as As-reducing if it carries any of the four arsenic reducing genes of *arsR*, *arsC* and *GstB* genes or as iron-reducing if it carries any of iron-reducing genes of *mtrA*, *mtrB* and *omcS*. Solid As concentration is 11.3 (4) mg/kg in YCA-1.5 m and 23.7 (15.2) mg/kg in YCA-11.2 m, respectively (P-extractable As in the parentheses). Genera with average relative abundance less than 1×10^{-4} are not shown. The genera have been previously reported for As/Iron reducing capability are labeled with red asterisk. (For interpretation of the references to color in this figure legend, the reader is referred to the web version of this article.)

Comamonas, *Delftia*, *Alicycliphilus* and *Bacillus* are evidently more abundant in YCA-11.2 m (bulk As concentration of 23.7 mg kg^{-1} and 36% of As is As(V)) than those in YCA-1.5 m (bulk As concentration of 11.3 mg kg^{-1} with 95% of As(V)). Arsenic reducing genera *Psychroflexus*, *Anaeromyxobacter* and *Shewanella* are prominent in YCA-1.5 m but are at very low prevalence ($< 10^{-4}$) in YCA-11.2 m. Similar to arsenic reducing genera, the abundance of iron reducing genera is higher (0.038%) for YCA-11.2 m and is lower (0.015%) for YCA-1.5 m. Additionally, high proportion of unclassified arsenic/iron reducing bacteria is identified in YCA-1.5 m, indicating not only the existence of novel arsenic/iron reducing metabolizer within the sediment microbiome but also a more diverse microbiome in the shallower sediment sample. The relative abundance of sulfate-reducing bacteria is 0.087% of YCA-11.2 m and 0.018% of YCA-0.5 m, respectively, supportive of the sulfate-reducing pockets observed in shallower depth zones at YCA (Table S7).

4. Discussion

4.1. Evidence for As mobilization by active reductive dissolution of As(V) bounded Fe(III) (hydr) oxides

Mobilization of As by reductive dissolution of its host in the sediments, i.e., Fe(III) (hydr)oxides has been widely accepted as the mechanism for elevated levels of geogenic As in groundwater of South and Southeast Asia, supported primarily by groundwater chemistry data (Smedley and Kinniburgh, 2002; Zheng et al., 2004). Laboratory adsorption experiments have shown that As adsorbed on ferrihydrite, goethite or complexed with Fe(III) nano-particles can possess a very high As:Fe molar ratio of 16–2000 mmol As per mol Fe (Dixit and Hering, 2003; Raven et al., 1998; Shi et al., 2020). Therefore, it is expected that oxidized As(V) adsorbed onto Fe(III) oxyhydroxides in suspended particulates prior to sedimentation constitutes a significant pool of mobilizable As in the aquifer sediments.

One of the most profound changes linked to redox state, is the change in As partitioning from the solid into solution. This results in a decrease in the solid-phase concentration of adsorbed As coincident with an increase in dissolved As levels. Paired Fe and As X-ray Spectroscopy measurements evaluating Fe mineralogy and As speciation allow us to quantify the molar ratios of adsorbed As(III) and As(V) to Fe(III) (hydr) oxides in sediments, and thus to evaluate the changes when redox changes occur, and to better quantify amounts of As that are bound to Fe phases. After excluding 16 samples with either below the practical detection limit of EXAFS linear combination fitting (5 mol% Fe) (Sun et al., 2018) or large uncertainties in linear combination fitting, it is clear that Fe(III) (hydr)oxides concentrations are higher in the 7 Fe/Mn-reducing sediments (0.24 ± 0.15 mol/kg) than in the 6 sulfate-reducing sediments (0.11 ± 0.04 mol/kg, Fig. 8 and Table S8), after excluding 4 As enriched samples. The sediment As(V)+As(III) concentrations are also significantly higher in the Fe/Mn-reducing

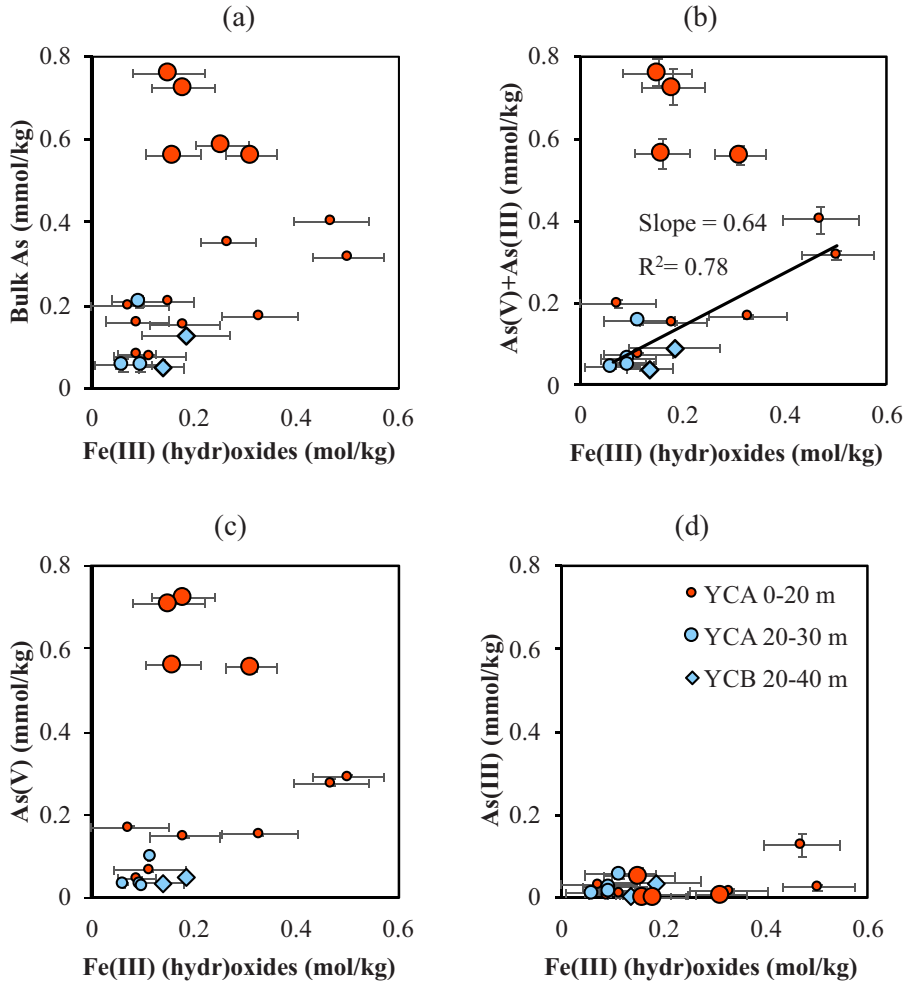

Fig. 8. The bulk As by XRF, As(V)+As(III), As(V) and As(III) concentrations from XANES vs Fe(III) (hydr)oxides concentration from amorphous and crystalline Fe(III) oxides by EXAFS in the sediments. Samples with Fe(III) (hydr)oxides fractions < 5% and large errors were excluded. Excluding 4 samples with superlative levels of As in (b), linear regression of 13 remaining data points finds 0.64 mmol of As(V)+As(III) for 1 mol of Fe(III) (hydr)oxides.

sections (0.19 ± 0.12 mmol/kg) than in the sulfate-reducing sections (0.08 ± 0.05 mmol/kg) (Mann–Whitney *U* test, Z = −2.14, $p = 0.03$). Furthermore, the concentration of sediment As(V)+As(III) correlates with that of Fe(III) (hydr)oxides, at a ratio of 0.64 mmol of As for 1 mol of Fe(III) (hydr)oxides in Yinchuan sediments ($R^2 = 0.72$, $p = 0.05$; Fig. 8b), after excluding the 4 very high-As samples. Similarly, in Hetao Basin located downstream from Yinchuan Plain that is also influenced by the Yellow River, a ratio of 0.9 mmol As (extracted by 0.1 M ascorbic acid, 0.2 M ammonium oxalate at pH 3, and 1 mM HCl leachate) per mol Fe(III) (hydr)oxides has been found in 8 aquifer sediments, with 54 ± 22 μmol kg^{-1} As and 0.06 ± 0.01 mol kg^{-1} Fe(III) (hydr)oxides (Qiao et al., 2020). The simultaneous decrease of sediment Fe(III) (hydr)oxides and As(V) concentrations (Fig. 8c), together with groundwater Fe and As being predominantly Fe(II) and As(III) (Table S3 and Fig. 2) and the presence of a diverse group of As(V) reducing genera (Fig. 7), provide direct evidence for active reductive dissolution of As(V) associated with Fe(III) (hydr)oxides as a mechanism for As mobilization.

We have compiled results from all 6 prior studies (Table S1) that reported paired As XANES and Fe EXAFS data on sediments from reducing aquifers, although sampled at a lower depth resolution of > 1.5 m per sample, from the Mekong River Delta (Quicksall et al., 2008; Stuckey et al., 2015), the Ganges–Brahmaputra–Meghna Delta in Bangladesh (Aziz et al., 2017; Gnanaprakasam et al., 2017; Mozumder et al., 2020) and the Jianghan Plain of the Yangtze River Delta (Schaefer et al., 2017). These prior studies show that the proportion of As(V) decreases with depth as the sediment becomes progressively more reducing but the As(V)+As(III) to Fe(III) (hydr)oxides ratios have not been systematically interpreted. The combination of paired As XANES and Fe EXAFS data reported in this study and in the literature offers several new insights on sediment As, its host Fe(III) (hydr)oxides and their intertwined transformation mediated by microbes. First, modern, organic-rich wetland sediments from the Mekong River delta (n = 12) and the Jianghan Plain (n = 2) appear to have the highest As(V)+As(III) to Fe(III) (hydr)oxides ratio of 0.99 ± 0.54 mmol As per mol Fe (Table S1) (Schaefer et al., 2017; Stuckey et al., 2015). This may be viewed as a plausible reference value for clayey sediment sections in the aquifer. Second, Holocene sediments from the Ganges–Brahmaputra Delta, the Mekong Delta, the Yangtze River and the Yellow River alluvial-fluvial plains have an intermediate As(V)+As(III) to Fe(III) (hydr)oxides ratio of 0.57 ± 0.47 mmol As per mol Fe with simultaneous decreases in sediment As(V) and Fe(III) (hydr)oxides concentrations with depth, reflecting progressively more reducing conditions (Fig. 8b, Tables S1 and S8). This is consistent with the reductive dissolution of As(V) loaded Fe(III) (hydr)oxides with progressively more reducing conditions at Yinchuan to result in a lowering of sediment As: Fe ratios. Third, although there are only limited data for confirmed or suspected Pleistocene sediments in Bangladesh and Cambodia (Table S1), the much lower As(V)+As(III) to Fe(III) (hydr)oxides ratio of 0.15 ± 0.09 mmol As per mol Fe, plus their higher Fe(III) (hydr)oxides concentration of 0.17– 0.42 mol kg^{-1}, supports that As in Pleistocene

sediments is less "mobilizable" than As in Holocene sediments (see Section 4.2). This low As:Fe ratio is likely due to flushing of As from such aquifers over several glacial-interglacial periods (van Geen et al., 2008) and oxidative weathering induced Fe(III) (hydr)oxides formation during enhanced flushing when sea levels are lower during glacial periods (Zheng et al., 2005). Finally, several samples are super-enriched in As. These super high-As sediments exhibit elevated ratios of adsorbed As to Fe(III) (hydr)oxides of 3.6 ± 1.2 mmol/mol ($n = 4$) relative to 1.0 ± 0.7 mmol/mol for other Fe/Mn-reducing sediments and 0.7 ± 0.3 mmol/mol for sulfate-reducing sediments ($p = 0.003$–0.01; Fig. 8b, Table S8). The elevated As: Fe(III) (hydr)oxides molar ratio of 3.8 ± 0.6 mmol/mol is also observed for 2 out of 5 sediment samples with superlative As of 88–108 mg kg^{-1} in reducing aquifer in Jianghan plain, while the rest 3 samples with As of 18.8 ± 5.0 mg kg^{-1} display much lower ratio of 1.2 ± 0.5 mmol As per mol Fe (Table S1) (Schaefer et al., 2017). The possible reasons for the As enrichment in sediment will be discussed further in Section 4.3.

4.2. Suppressed reduction of As(V) and iron(III) oxides in organic-poor sediments

Sediment organic matter is consumed with reduction and mobilization of sediment As at our study sites in Yinchuan. Sulfate reducing sediment sections contain less TOC ($0.04\% \pm 0.02\%$) and As(V) ($52\% \pm 17\%$, 2.6 ± 1.3 mg kg^{-1}), compared with the Fe/Mn reducing sediment sections with $0.09\% \pm 0.11\%$ of TOC and $72\% \pm 19\%$ or 9.2 ± 6.1 mg kg^{-1} of As(V) after excluding the 7 samples with superlative levels of As. Furthermore, the aquifer sediments in Yinchuan are characterized by low organic carbon, in comparison with other As-contaminated reducing aquifers of the Yellow River corridor: mean TOC is 0.6% (0.28–1.30, n = 12) in Datong Basin (Xie et al., 2008) and 0.35% (0.03–1.65, n = 66) in Hetao Basin (Shen et al., 2018). The TOC content of Bangladesh Holocene sediments ranges from 0.08% to 0.4% (Zheng et al., 2005; Swartz et al., 2004; Reza et al., 2010a). The result of reactive transport modeling based on field data from the Red River Delta, Vietnam suggests that the declining rate of organic carbon degradation over time has caused decreasing rate of Fe oxides dissolution containing As(V), with simultaneous decreases in groundwater As (Postma et al., 2016). Recently, a 100-day microcosm study suggests the rate of Fe(III) mineral reduction is much slower with *in situ* organic carbon extracted from sandy aquifer sediments from Vietnam, than that amended with simple labile model carbon sources acetate and lactate (Glodowska et al., 2020). Field investigation in Hetao basin has found where groundwater As concentration is high, depth-matched sediments usually contain higher fractions of biodegradable organic carbon (Qiao et al., 2020). The enhanced As mobility with increasing quantity of biodegradable TOC is further demonstrated by batch incubation experiment, which shows that 1.0–1.64 μmol/L As is released during incubation from sediments containing a higher TOC concentration of 0.15% and presumably more bioavailable carbon (as lipids, aliphatic/proteins, and carbohydrates, of molecules with $H/C \geq 1.5$). In comparison, only 0.2 μmol/L As is released from sediments containing a lower TOC of 0.11% and less bioavailable carbon (Qiao et al., 2020). Taken together, the presence of As(V)-Fe(III) minerals and the low TOC content in sulfate reducing sediments in Yinchuan Plain suggest that the rate of microbial As(V) reduction is limited by the quantity and the quality (bioavailability) of sediment organic carbon.

Two of the most abundant As reducing genera identified in our metagenome analysis, *Bacillus* and *Pseudomonas*, are also identified and isolated from high-As aquifer sediments in Hetao Basin using 16S rRNA gene and As marker gene (Guo et al., 2015). The Hetao Basin clay sediment with predominantly As(V) releases ~15% of total solid As into solution to reach 200 μg/L of As, most as As(III), twice higher in the presence of As reducing bacteria (*Bacillus sp*. M17-15 and *Pseudomonas sp*. M17-1) at the end of the 14-day incubation experiment than in the control (Guo et al., 2015). Compared to Yinchuan sediment, it is likely that the more intense microbial reduction observed in Hetao Basin is due to more abundant microbes and organic carbon that are more bioavailable. Nevertheless, the higher Fe, As and S reducing bacteria in YCA-11.2 m than those in YCA-0.5 m leaves the possibility for such microbes to play a role in As mobilization. However, further investigations such as incubation experiments with addition of labile carbon and/or amendments with isolated microbes are needed to provide constraints on mineralogical transformation observed in the high depth resolution sampling here in (Fig. 1). Another especially relevant investigation is an elegant incubation experiment conducted using a Pleistocene sediment sample (depth: 43.3–43.9 m) from site A of Araihazar, Bangladesh (Dhar et al., 2011). This sediment sample initially contains a 1-hr hot HCl-leachable Fe concentration of 0.79 ± 0.15 g kg^{-1} and phosphate-extractable As concentration of 0.14 ± 0.03 mg kg^{-1}, mostly (> 95%) in the form of Fe(III) and As(III), respectively. Incubated with 50 mg/L of lactate and *Shewanella* sp. strain ANA-3 inoculation, even with addition of an antibiotic, this sediment sample releases As to 17.3 ± 3.7 μg/L with 80% being As(III) after only 23 days. Most importantly, the sediment sample shows significantly altered Fe and As mineralogical compositions: not only the color changes from orange to gray, but also the hot HCl-leachable Fe concentration increases to 5.4 ± 0.04 g kg^{-1} with only 20% being Fe(III), with simultaneous increase in P-extractable As to 0.56 ± 0.01 mg kg^{-1} with 57% being As (III). Although microbiome data are obtained on only two sediment samples in this study, *Shewanella* and other Fe reducing bacteria are consistently identified in both of them (Fig. 7). Therefore, one might expect similar mineralogical transformation as observed in Dhar et al. (2011) if Fe/Mn reducing sediments in our sediment cores were incubated with lactate and *Shewanella* sp., although natural organic matter degradation and reduction that took place over geologic time scales could occur through other pathways.

4.3. Enrichment of geogenic arsenic in Yinchuan Plain sediment

Of all 75 sediment samples in this study, 47% contain bulk As concentrations greater than the Upper Crustal As abundance of 5.7 mg kg^{-1} (Hu and Gao, 2008), with 7 samples containing exceptionally high As concentrations (> 65 mg kg^{-1}, Table S6 and Fig. 4). Occasionally, such high As levels (up to 80 mg kg^{-1}) have also been reported from other sites in Yinchuan (Guo et al., 2014), suggesting that these enrichments are not restricted to this field site. These high As concentrations are likely geogenic, they are stratigraphically bound by low-As sediment above and below, and are found at rural, agricultural study sites with no known industrial activities that could pollute the sediments with As. Furthermore, sediment As loading by irrigation with As-contaminated groundwater over a period of 60-years is estimated to be only 0.5 mg kg^{-1}. The estimation assumes that the irrigation rate is 2 mm/day for 60 days a year (Liu et al., 2018), that the groundwater contains 200 μg L^{-1} As, and that the irrigated As is distributed uniformly in the top 3 m of the sediments with a density of 2 g cm^{-3} and a porosity of 0.25. Because the bulk Fe and Si/Al ratios of YCA and YCB sediments are comparable with those of the Yellow River sediments (Fig. 6), they likely share a common geogenic origin. The Yellow River sediments come from an extensive watershed containing widely variable As levels, but are usually lower though they can show evidence of modest enrichment up to ~ 30 mg kg^{-1} As (Fig. 6, Table S9) (Pang et al., 2018; Zhou et al., 2015). In Eastern Tibet, the headwater regions of the Yellow River, top soil contains up to 154 mg kg^{-1} of As, but the average As concentration is far lower at 21.5 ± 24.5 mg kg^{-1} ($n = 39$, Table S9) (Sheng et al., 2012). Concentrations of As in modern suspended particles averaged 33 ± 11 ($n = 16$) and 17 ± 2 ($n = 6$) for the upper (Lanzhou) and middle (Xiaolangdi Reservoir outlet) stretches of the Yellow River, respectively (Liu et al., 2009; Dong et al., 2019). Therefore, high-As sediments at this site appear to have resulted from local processes that enrich As relative to levels found in sediments following deposition.

These super-enrichment of sediment As concentrations are likely due

to redox trapping of groundwater As in past zones of groundwater discharge. When reducing groundwater with high concentrations of dissolved As and Fe flow through the oxic or suboxic hyporheic zone, the discharging As can be trapped by freshly precipitated ferrihydrite from oxidation of groundwater Fe^{2+}, resulting in superlative levels of As that are highly localized both vertically (5 cm – 3 m) and horizontally (12–500 m) in sediments – this mechanism has been verified by several studies along the Meghna River (Jung et al., 2012, 2015; Datta et al., 2009), as well as from the Waquoit Bay (Jung et al., 2009). Redox trapping of As in the now-buried hyporheic zone along groundwater discharge flow path may have also occurred in Yinchuan Plain (Fig. 1). Within our cores, high sediment As concentrations are encountered in 7 samples out of a total of 75 samples. Specifically, 5 samples from YCA (depth: 14.5, 15.3, 16.6, 17.2 and 17.6 m) contain bulk As of 42, 44, 42, 54 and 57 mg kg^{-1} and phosphate-extractable As of 43, 51, 52, 31 and 100 mg kg^{-1} (Table S6); 2 samples from YCB (depth 1.5 and 2.5 m) contain bulk As of 123 and 133 mg kg^{-1}, with phosphate-extractable As of 73.4 mg kg^{-1} for YCB-2.5 m (Table S6). The observation that the amount of phosphate-extractable As exceeds bulk As at YCA can be attributed to large sediment heterogeneity at cm scale because the samples for the two measurements that are intended to be replicates are in reality a few cm apart. Second, in these As super-enriched samples, As (V) dominates (92 ± 13%, n = 5). Third, these samples contain high fractions of amorphous and crystalline Fe(III) (hydr)oxides at 35 ± 9% (n = 5), with concentrations of 12 ± 3 g kg^{-1} (Tables S4 and S5). In comparison, X-ray Absorption Spectroscopy analysis of Meghna riverbank sediment samples has found a roughly 50–50 mix of As(III)-As(V), with ferrihydrite-like Fe(III) phase accounting for 49 ± 8% of Fe minerals in the As enriched-layers (depth < 2 m) (Jung et al., 2012, 2015).

To accumulate so much As in sediments by groundwater discharge, it requires substantial time. Here, we have estimated the time required to reach measured sediment As concentrations following the method of Jung et al. (2015). The distribution coefficient (K_d) ranges from 14 to 26 L kg^{-1} for high As groundwater samples ([As] >10 μg L^{-1}, n = 5), as estimated by depth-matched dissolved As and P-extractable As concentrations. Assuming a porosity of 0.25, a sediment bulk density of 2 g cm^{-3} and a groundwater flow rate of 20 m y^{-1} typical of the unconfined aquifer in Yinchuan (Han et al., 2013), the groundwater velocities are calculated to be 1.4 and 0.8 m yr^{-1} with retardation factors being 113 and 209 for K_d of 14 and 26 L kg^{-1}, respectively; equivalent to 5600–10,500 years to accumulate ~100 mg kg^{-1} of As in a 1-m sediment section. For comparison, approximately 350–2600 years are required to accumulate As within the top 5–10 cm layer of the Meghna riverbanks where it has been documented previously (Jung et al., 2015). It is thus reasonable for Holocene or older Yinchuan Plain sediments to accumulate As to measured levels, though that accumulation would likely have occurred over much of that sediment's lifetime.

CRediT authorship contribution statement

Yuqin Sun: Investigation, Methodology, Formal analysis, Writing - Original draft preparation, Writing - Review & Editing; **Jing Sun:** Methodology, Writing - Review & Editing; **Athena Nghiem:** Investigation, Writing - Review & Editing; **Benjamin Bostick:** Investigation, Methodology, Writing - Review & Editing, Funding acquisition; **Tyler Ellis:** Investigation; **Long Han:** Investigation, Methodology; **Zengyi Li:** Investigation, Methodology; **Songlin Liu:** Investigation; **Shuangbao Han**: Investigation; **Miao Zhang**: Methodology, Formal analysis; **Yu Xia**: Methodology, Writing - Review & Editing; **Yan Zheng**: Conceptualization, Investigation, Methodology, Writing- Original draft preparation, Writing - Review & Editing, Supervision and Funding acquisition.

Declaration of Competing Interest

The authors declare that they have no known competing financial interests or personal relationships that could have appeared to influence the work reported in this paper.

Data availability

All data are archived online (http://opendata.pku.edu.cn/dataverse/yinchuan) and presented in supporting information.

Acknowledgments

Funding for this work was provided by the National Natural Science Foundation of China Grant 41772265 and 41831279 and Shenzhen Science and Technology Innovation Commission Grant GJHZ20180411143520274 to Y.Z., and National Science Foundation (NSF) grant EAR 15-21356, National Institute of Environmental Health Sciences grant ES010349 to B.C.B., and an NSF Graduate Research Fellowship to A.A.N. We thank Tingwen Wu from CGS and Yunjie Ma, Meng Ma from Y.Z.'s lab for their help with the fieldwork; Zhenjie Zhao and Shehong Li from Institute of Geochemistry of CAS for grain size analysis; Yating Shen from Chinese Academy of Geological Sciences and Zhen Tan for valuable discussion. This research used resources of the Stanford Synchrotron Radiation Light source, SLAC National Accelerator Laboratory, is supported by the U.S. Department of Energy, Office of Science, Office of Basic Energy Sciences under Contract No. DE-AC02-76SF00515.

Appendix A. Supporting information

Supplementary data associated with this article can be found in the online version at doi:10.1016/j.jhazmat.2020.124615.

References

Allen, H.E., Fu, G., Deng, B., 1993. Analysis of acid-volatile sulfide (AVS) and simultaneously extracted metals (SEM) for the estimation of potential toxicity in aquatic sediments. Environ. Toxicol. Chem. 12, 1441–1453.
Amen, R., Bashir, H., Bibi, I., Shaheen, S.M., Niazi, N.K., Shahid, M., Hussain, M.M., Antoniadis, V., Shakoor, M.B., Al-Solaimani, S.G., Wang, H., Bundschuh, J., Rinklebe, J., 2020. A critical review on arsenic removal from water using biochar-based sorbents: the significance of modification and redox reactions. Chem. Eng. J. 396, 125195.
Anderson, M.P., Aiken, J.S., Webb, E.K., Mickelson, D.M., 1999. Sedimentology and hydrogeology of two braided stream deposits. Sediment. Geol. 129, 187–199.
Antoniadis, V., Shaheen, S.M., Levizou, E., Shahid, M., Niazi, N.K., Vithanage, M., Ok, Y. S., Bolan, N., Rinklebe, J., 2019. A critical prospective analysis of the potential toxicity of trace element regulation limits in soils worldwide: are they protective concerning health risk assessment? - A review. Environ. Int. 127, 819–847.
Aziz, Z., Bostick, B.C., Zheng, Y., Huq, M.R., Rahman, M.M., Ahmed, K.M., van Geen, A., 2017. Evidence of decoupling between arsenic and phosphate in shallow groundwater of Bangladesh and potential implications. Appl. Geochem. 77, 167–177.
Berg, M., Tran, H.C., Nguyen, T.C., Pham, H.V., Schertenleib, R., Giger, W., 2001. Arsenic contamination of groundwater and drinking water in Vietnam: a human health threat. Environ. Sci. Technol. 35, 2621–2626.
Bolger, A.M., Lohse, M., Usadel, B., 2014. Trimmomatic: a flexible trimmer for Illumina sequence data. Bioinformatics 30, 2114–2120.
Bostick, B.C., Chen, C., Fendorf, S., 2004. Arsenite retention mechanisms within estuarine sediments of Pescadero, CA. Environ. Sci. Technol. 38, 3299–3304.
Bowell, R.J., 1994. Sorption of arsenic by iron oxides and oxyhydroxides in soils. Appl. Geochem. 9, 279–286.
Cheng, Z., Zheng, Y., Mortlock, R., van Geen, A., 2004. Rapid multi-element analysis of groundwater by high-resolution inductively coupled plasma mass spectrometry. Anal. Bioanal. Chem. 379, 512–518.
Dang, C.Y., Xia, Y., Zheng, M.S., Liu, T., Liu, W., Chen, Q., Ni, J.R., 2020. Metagenomic insights into the profile of antibiotic resistomes in a large drinking water reservoir. Environ. Int. 136, 105449.
Datta, S., Mailloux, B., Jung, H.B., Hoque, M.A., Stute, M., Ahmed, K.M., Zheng, Y., 2009. Redox trapping of arsenic during groundwater discharge in sediments from the Meghna riverbank in Bangladesh. Proc. Natl. Acad. Sci. USA 106, 16930–16935.
Dhar, R.K., Zheng, Y., Saltikov, C.W., Radloff, K.A., Mailloux, B.J., Ahmed, K.M., van Geen, A., 2011. Microbes enhance mobility of arsenic in pleistocene aquifer sand from Bangladesh. Environ. Sci. Technol. 45, 2648–2654.
Dixit, S., Hering, J.G., 2003. Comparison of arsenic(V) and arsenic(III) sorption onto iron oxide minerals: implications for arsenic mobility. Environ. Sci. Technol. 37, 4182–4189.
Dong, J., Xia, X., Liu, Z., Zhang, X., Chen, Q., 2019. Variations in concentrations and bioavailability of heavy metals in rivers during sediment suspension-deposition

event induced by dams: insights from sediment regulation of the Xiaolangdi Reservoir in the Yellow River. J. Soils Sediment. 19, 403–414.
Fendorf, S., Michael, H.A., van Geen, A., 2010. Spatial and temporal variations of groundwater arsenic in south and southeast Asia. Science 328, 1123–1127.
Frohne, T., Rinklebe, J., Diaz-Bone, R.A., Du Laing, G., 2011. Controlled variation of redox conditions in a floodplain soil: impact on metal mobilization and biomethylation of arsenic and antimony. Geoderma 160, 414–424.
Garber, A.I., Nealson, K.H., Okamoto, A., McAllister, S.M., Chan, C.R.S., Barco, R.A., Merino, N., 2020. FeGenie: a comprehensive tool for the identification of iron genes and iron gene neighborhoods in genome and metagenome assemblies. Front. Microbiol. 11.
Van Geen, A., Rose, J., Thoral, S., Garnier, J.M., Zheng, Y., Bottero, J.Y., 2004. Decoupling of As and Fe release to Bangladesh groundwater under reducing conditions. Part II: evidence from sediment incubations. Geochim. Cosmochim. Acta 68, 3475–3486.
van Geen, A., Zheng, Y., Goodbred Jr., S., Horneman, A., Aziz, Z., Cheng, Z., Stute, M., Mailloux, B., Weinman, B., Hoque, M.A., Seddique, A.A., Hossain, M.S., Chowdhury, S.H., Ahmed, K.M., 2008. Flushing history as a hydrogeological control on the regional distribution of arsenic in shallow groundwater of the Bengal Basin. Environ. Sci. Technol. 42, 2283–2288.
van Geen, A., Zheng, Y., Versteeg, R., Stute, M., Horneman, A., Dhar, R., Steckler, M., Gelman, A., Small, C., Ahsan, H., Graziano, J.H., Hussain, I., Ahmed, K.M., 2003. Spatial variability of arsenic in 6000 tube wells in a 25 km(2) area of Bangladesh. Water Resour. Res. 39.
Glodowska, M., Stopelli, E., Schneider, M., Lightfoot, A., Rathi, B., Straub, D., Patzner, M., Duyen, V.T., Berg, M., Kleindienst, S., Kappler, A., AdvectAs Team, M., 2020. Role of in situ natural organic matter in mobilizing as during microbial reduction of Fe-III-mineral-bearing aquifer sediments from Hanoi (Vietnam). Environ. Sci. Technol. 54, 4149–4159.
Gnanaprakasam, E.T., Lloyd, J.R., Boothman, C., Ahmed, K.M., Choudhury, I., Bostick, B. C., van Geen, A., Mailloux, B.J., 2017. Microbial community structure and arsenic biogeochemistry in two arsenic-impacted aquifers in Bangladesh. Mbio 8.
Goodbred, S.L., Kuehl, S.A., 2000. The significance of large sediment supply, active tectonism, and eustasy on margin sequence development: late Quaternary stratigraphy and evolution of the Ganges-Brahmaputra delta. Sediment. Geol. 133, 227–248.
Guo, Q., Guo, H., Yang, Y., Han, S., Zhang, F., 2014. Hydrogeochemical contrasts between low and high arsenic groundwater and its implications for arsenic mobilization in shallow aquifers of the northern Yinchuan Basin, P.R. China. J. Hydrol. 518, 464–476.
Guo, H., Liu, Z., Ding, S., Hao, C., Xiu, W., Hou, W., 2015. Arsenate reduction and mobilization in the presence of indigenous aerobic bacteria obtained from high arsenic aquifers of the Hetao basin, Inner Mongolia. Environ. Pollut. 203, 50–59.
Han, S., Zhang, F., Zhang, H., An, Y., Wang, Y., Wu, X., Wang, C., 2013. Spatial and temporal patterns of groundwater arsenic in shallow and deep groundwater of Yinchuan Plain, China. J. Geochem. Explor. 135, 71–78.
Hao, Q., Wang, L., Oldfield, F., Peng, S., Qin, L., Song, Y., Xu, B., Qiao, Y., Bloemendal, J., Guo, Z., 2012. Delayed build-up of Arctic ice sheets during 400,000-year minima in insolation variability. Nature 490, 393–396.
Harvey, C.F., Swartz, C.H., Badruzzaman, A.B.M., Keon-Blute, N., Yu, W., Ali, M.A., Jay, J., Beckie, R., Niedan, V., Brabander, D., Oates, P.M., Ashfaque, K.N., Islam, S., Hemond, H.F., Ahmed, M.F., 2002. Arsenic mobility and groundwater extraction in Bangladesh. Science 298, 1602–1606.
Horneman, A., Van Geen, A., Kent, D.V., Mathe, P.E., Zheng, Y., Dhar, R.K., O'Connell, S., Hoque, M.A., Aziz, Z., Shamsudduha, M., Seddique, A.A., Ahmed, K. M., 2004. Decoupling of As and Fe release to Bangladesh groundwater under reducing conditions. Part 1: evidence from sediment profiles. Geochim. Cosmochim. Acta 68, 3459–3473.
Hussain, M.M., Wang, J., Bibi, I., Shahid, M., Niazi, N.K., Iqbal, J., Mian, I.A., Shaheen, S. M., Bashir, S., Shah, N.S., Hina, K., Rinklebe, J., 2021. Arsenic speciation and biotransformation pathways in the aquatic ecosystem: the significance of algae. J. Hazard. Mater. 403, 124027.
Hu, Z., Gao, S., 2008. Upper crustal abundances of trace elements: a revision and update. Chem. Geol. 253, 205–221.
Hyatt, D., Chen, G.L., LoCascio, P.F., Land, M.L., Larimer, F.W., Hauser, L.J., 2010. Prodigal: prokaryotic gene recognition and translation initiation site identification. BMC Bioinform. 11, 119.
Ji, G., Silver, S., 1992. Reduction of arsenate to arsenite by the ArsC protein of the arsenic resistance operon of Staphylococcus aureus plasmid pI258. Proc. Natl. Acad. Sci. USA 89, 9474–9478.
Jung, H.B., Bostick, B.C., Zheng, Y., 2012. Field, experimental, and modeling study of arsenic partitioning across a redox transition in a Bangladesh aquifer. Environ. Sci. Technol. 46, 1388–1395.
Jung, H.B., Charette, M.A., Zheng, Y., 2009. Field, laboratory, and modeling study of reactive transport of groundwater arsenic in a coastal aquifer. Environ. Sci. Technol. 43, 5333–5338.
Jung, H.B., Zheng, Y., 2006. Enhanced recovery of arsenite sorbed onto synthetic oxides by L-ascorbic acid addition to phosphate solution: calibrating a sequential leaching method for the speciation analysis of arsenic in natural samples. Water Res. 40, 2168–2180.
Jung, H.B., Zheng, Y., Rahman, M.W., Rahman, M.M., Ahmed, K.M., 2015. Redox zonation and oscillation in the hyporheic zone of the Ganges-Brahmaputra-Meghna Delta: implications for the fate of groundwater arsenic during discharge. Appl. Geochem. 63, 647–660.
Kocar, B.D., Fendorf, S., 2009. Thermodynamic constraints on reductive reactions influencing the biogeochemistry of arsenic in soils and sediments. Environ. Sci. Technol. 43, 4871–4877.
Kocar, B.D., Polizzotto, M.L., Benner, S.G., Ying, S.C., Ung, M., Ouch, K., Samreth, S., Suy, B., Phan, K., Sampson, M., Fendorf, S., 2008. Integrated biogeochemical and hydrologic processes driving arsenic release from shallow sediments to groundwaters of the Mekong delta. Appl. Geochem. 23, 3059–3071.
Kumarathilaka, P., Seneweera, S., Meharg, A., Bundschuh, J., 2018. Arsenic speciation dynamics in paddy rice soil-water environment: sources, physico-chemical, and biological factors - A review. Water Res. 140, 403–414.
Kumar, N., Noël, V., Planer-Friedrich, B., Besold, J., Lezama-Pacheco, J., Bargar, J.R., Brown, G.E., Fendorf, S., Boye, K., 2020. Redox heterogeneities promote thioarsenate formation and release into groundwater from low arsenic sediments. Environ. Sci. Technol. 54, 3237–3244.
Du Laing, G., Chapagain, S.K., Dewispelaere, M., Meers, E., Kazama, F., Tack, F.M.G., Rinklebe, J., Verloo, M.G., 2009. Presence and mobility of arsenic in estuarine wetland soils of the Scheldt estuary (Belgium). J. Environ. Monit. 11, 873–881.
Lascelles, J., Burke, K.A., 1978. Reduction of ferric iron by L-lactate and DL-glycerol-3-phosphate in membrane preparations from Staphylococcus aureus and interactions with the nitrate reductase system. J. Bacteriol. 134, 585–589.
LeMonte, J.J., Stuckey, J.W., Sanchez, J.Z., Tappero, R., Rinklebe, J., Sparks, D.L., 2017. Sea level rise induced arsenic release from historically contaminated coastal soils. Environ. Sci. Technol. 51, 5913–5922.
Liao, V.H.-C., Chu, Y.-J., Su, Y.-C., Hsiao, S.-Y., Wei, C.-C., Liu, C.-W., Liao, C.-M., Shen, W.-C., Chang, F.-J., 2011. Arsenite-oxidizing and arsenate-reducing bacteria associated with arsenic-rich groundwater in Taiwan. J. Contam. Hydrol. 123, 20–29.
Liu, M., Jiang, Y., Xu, X., Huang, Q., Huo, Z., Huang, G., 2018. Long-term groundwater dynamics affected by intense agricultural activities in oasis areas of arid inland river basins, Northwest China. Agric. Water Manag. 203, 37–52.
Liu, C., Xu, J., Liu, C., Zhang, P., Dai, M., 2009. Heavy metals in the surface sediments in Lanzhou Reach of Yellow River, China. Bull. Environ. Contam. Toxicol. 82, 26–30.
Meng, X., Korfiatis, G.P., Jing, C., Christodoulatos, C., 2001. Redox transformations of arsenic and iron in water treatment sludge during aging and TCLP extraction. Environ. Sci. Technol. 35, 3476–3481.
Mozumder, M.R.H., Bostick, B.C., Selim, M., Islam, M.A., Shoenfelt, E.M., Ellis, T., Mailloux, B.J., Choudhury, I., Ahmed, K.M., van Geen, A., 2020. Similar retardation of arsenic in gray Holocene and orange Pleistocene sediments: evidence from field-based column experiments in Bangladesh. Water Res. 183, 116081.
Natasha, I. Bibi, Shahid, M., Niazi, N.K., Younas, F., Naqvi, S.R., Shaheen, S.M., Imran, M., Wang, H., Hussaini, K.M., Zhang, H., Rinklebe, J., 2021. Hydrogeochemical and health risk evaluation of arsenic in shallow and deep aquifers along the different floodplains of Punjab, Pakistan. J. Hazard. Mater. 402, 124074.
Nickson, R.T., McArthur, J.M., Ravenscroft, P., Burgess, W.G., Ahmed, K.M., 2000. Mechanism of arsenic release to groundwater, Bangladesh and West Bengal. Appl. Geochem. 15, 403–413.
O'Day, P.A., Rivera, N., Root, R., Carroll, S.A., 2004b. X-ray absorption spectroscopic study of Fe reference compounds for the analysis of natural sediments. Am. Mineral. 89, 572–585.
O'Day, P.A., Vlassopoulos, D., Root, R., Rivera, N., 2004a. The influence of sulfur and iron on dissolved arsenic concentrations in the shallow subsurface under changing redox conditions. Proc. Natl. Acad. Sci. USA 101, 13703–13708.
Pang, H., Pan, B., Garzanti, E., Gao, H., Zhao, X., Chen, D., 2018. Mineralogy and geochemistry of modern Yellow River sediments: implications for weathering and provenance. Chem. Geol. 488, 76–86.
Podgorski, J., Berg, M., 2020. Global threat of arsenic in groundwater. Science 368, 845–850.
Postma, D., Jessen, S., Nguyen Thi Minh, H., Mai Thanh, D., Koch, C.B., Pham Hung, V., Pham Quy, N., Larsen, F., 2010. Mobilization of arsenic and iron from Red River floodplain sediments, Vietnam. Geochim. Cosmochim. Acta 74, 3367–3381.
Postma, D., Pham, T.K.T., Sø, H.U., Hoang, V.H., Vi, M.L., Nguyen, T.T., Larsen, F., Pham, H.V., Jakobsen, R., 2016. A model for the evolution in water chemistry of an arsenic contaminated aquifer over the last 6000years, Red River floodplain, Vietnam. Geochim. Cosmochim. Acta 195, 277–292.
Qiao, W., Guo, H., He, C., Shi, Q., Xiu, W., Zhao, B., 2020. Molecular evidence of arsenic mobility linked to biodegradable organic matter. Environ. Sci. Technol. 54, 7280–7290.
Quicksall, A.N., Bostick, B.C., Sampson, M.L., 2008. Linking organic matter deposition and iron mineral transformations to groundwater arsenic levels in the Mekong delta, Cambodia. Appl. Geochem. 23, 3088–3098.
Radloff, K.A., Zheng, Y., Stute, M., Weinman, B., Bostick, B., Mihajlov, I., Bounds, M., Rahman, M.M., Huq, M.R., Ahmed, K.M., Schlosser, P., van Geen, A., 2017. Reversible adsorption and flushing of arsenic in a shallow, Holocene aquifer of Bangladesh. Appl. Geochem. 77, 142–157.
Raven, K.P., Jain, A., Loeppert, R.H., 1998. Arsenite and arsenate adsorption on ferrihydrite: kinetics, equilibrium, and adsorption envelopes. Environ. Sci. Technol. 32, 344–349.
Reza, A.H.M.S., Jean, J.-S., Lee, M.-K., Liu, C.-C., Bundschuh, J., Yang, H.-J., Lee, J.-F., Lee, Y.-C., 2010a. Implications of organic matter on arsenic mobilization into groundwater: evidence from northwestern (Chapai-Nawabganj), central (Manikganj) and southeastern (Chandpur) Bangladesh. Water Res. 44, 5556–5574.
Reza, A.H.M.S., Jean, J.-S., Lee, M.-K., Yang, H.-J., Liu, C.-C., 2010b. Arsenic enrichment and mobilization in the Holocene alluvial aquifers of the Chapai-Nawabganj district, Bangladesh: a geochemical and statistical study. Appl. Geochem. 25, 1280–1289.
Schaefer, M.V., Guo, X., Gan, Y., Benner, S.G., Griffin, A.M., Gorski, C.A., Wang, Y., Fendorf, S., 2017. Redox controls on arsenic enrichment and release from aquifer sediments in central Yangtze River Basin. Geochim. Cosmochim. Acta 204, 104–119.

Schumacher, B.A., 2002. Methods for the determination of total organic carbon (TOC) in soils and sediments.
Seemann, T., 2014. Prokka: rapid prokaryotic genome annotation. Bioinformatics 30, 2068–2069.
Shah, R., Jha, S., 2013. Alishewanella sp. strain GIDC-5, Arsenite hyper-tolerant bacteria isolated from industrial effluent of South Gujarat, India. Chem. Ecol. 29, 427–436.
Shakoor, M.B., Niazi, N.K., Bibi, I., Shahid, M., Saqib, Z.A., Nawaz, M.F., Shaheen, S.M., Wang, H., Tsang, D.C.W., Bundschuh, J., Ok, Y.S., Rinklebe, J., 2019. Exploring the arsenic removal potential of various biosorbents from water. Environ. Int. 123, 567–579.
Sheng, J., Wang, X., Gong, P., Tian, L., Yao, T., 2012. Heavy metals of the Tibetan top soils Level, source, spatial distribution, temporal variation and risk assessment. Environ. Sci. Pollut. Res. 19, 3362–3370.
Shen, M., Guo, H., Jia, Y., Cao, Y., Zhang, D., 2018. Partitioning and reactivity of iron oxide minerals in aquifer sediments hosting high arsenic groundwater from the Hetao basin, P. R. China. Appl. Geochem. 89, 190–201.
Shi, Q., Sterbinsky, G.E., Zhang, S., Christodoulatos, C., Korfiatis, G.P., Meng, X., 2020. Formation of Fe(iii)–As(v) complexes: effect on the solubility of ferric hydroxide precipitates and molecular structural identification. Environ. Sci. Nano 7, 1388–1398.
Smedley, P.L., Kinniburgh, D.G., 2002. A review of the source, behaviour and distribution of arsenic in natural waters. Appl. Geochem. 17, 517–568.
Smedley, P.L., Kinniburgh, D.G., Macdonald, D.M.J., Nicolli, H.B., Barros, A.J., Tullio, J. O., Pearce, J.M., Alonso, M.S., 2005. Arsenic associations in sediments from the loess aquifer of La Pampa, Argentina. Appl. Geochem. 20, 989–1016.
Stuckey, J.W., Schaefer, M.V., Benner, S.G., Fendorf, S., 2015. Reactivity and speciation of mineral-associated arsenic in seasonal and permanent wetlands of the Mekong Delta. Geochim. Cosmochim. Acta 171, 143–155.
Sun, J., Chillrud, S.N., Mailloux, B.J., Stute, M., Singh, R., Dong, H., Lepre, C.J., Bostick, B.C., 2016. Enhanced and stabilized arsenic retention in microcosms through the microbial oxidation of ferrous iron by nitrate. Chemosphere 144, 1106–1115.
Sun, J., Mailloux, B.J., Chillrud, S.N., van Geen, A., Thompson, A., Bostick, B.C., 2018. Simultaneously quantifying ferrihydrite and goethite in natural sediments using the method of standard additions with X-ray absorption spectroscopy. Chem. Geol. 476, 248–259.
Swartz, C.H., Blute, N.K., Badruzzman, B., Ali, A., Brabander, D., Jay, J., Besancon, J., Islam, S., Hemond, H.F., Harvey, C.F., 2004. Mobility of arsenic in a Bangladesh aquifer: inferences from geochemical profiles, leaching data, and mineralogical characterization. Geochim. Cosmochim. Acta 68, 4539–4557.
Wallis, I., Prommer, H., Berg, M., Siade, A.J., Sun, J., Kipfer, R., 2020. The river–groundwater interface as a hotspot for arsenic release. Nat. Geosci. 13, 288–295.
Wang, J., Shen, M., Hu, J., Wei, M., Zhao, X., Liu, S., Li, X., Li, X., 2015. Magnetostratigraphy and its paleoclimatic significance of the PL02 borehole in the Yinchuan Basin. J. Asian Earth Sci. 114, 258–265.
Webb, S.M., 2005. SIXPack a graphical user interface for XAS analysis using IFEFFIT. Phys. Scr. 1011–1014.
Wood, D.E., Salzberg, S.L., 2014. Kraken: ultrafast metagenomic sequence classification using exact alignments. Genome Biol. 15, R46.
Xie, X., Wang, Y., Su, C., Liu, H., Duan, M., Xie, Z., 2008. Arsenic mobilization in shallow aquifers of Datong Basin: hydrochemical and mineralogical evidences. J. Geochem. Explor. 98, 107–115.
Yang, Q., Culbertson, C.W., Nielsen, M.G., Schalk, C.W., Johnson, C.D., Marvinney, R.G., Stute, M., Zheng, Y., 2015. Flow and sorption controls of groundwater arsenic in individual boreholes from bedrock aquifers in central Maine, USA. Sci. Total Environ. 505, 1291–1307.
Yang, Q., Tu, S., Wang, G., Liao, X., Yan, X., 2012. Effectiveness of applying arsenate reducing bacteria to enhance arsenic removal from polluted soils by Pteris vittata L. Int. J. Phytoremediat. 14, 89–99.
Zheng, Y., Stute, M., van Geen, A., Gavrieli, I., Dhar, R., Simpson, H.J., Schlosser, P., Ahmed, K.M., 2004. Redox control of arsenic mobilization in Bangladesh groundwater. Appl. Geochem. 19, 201–214.
Zheng, Y., van Geen, A., Stute, M., Dhar, R., Mo, Z., Cheng, Z., Horneman, A., Gavrieli, I., Simpson, H.J., Versteeg, R., Steckler, M., Grazioli-Venier, A., Goodbred, S., Shahnewaz, M., Shamsudduha, M., Hoque, M.A., Ahmed, K.M., 2005. Geochemical and hydrogeological contrasts between shallow and deeper aquifers in two villages of Araihazar, Bangladesh: implications for deeper aquifers as drinking water sources. Geochim. Cosmochim. Acta 69, 5203–5218.
Zhou, X., Li, A., Jiang, F., Lu, J., 2015. Effects of grain size distribution on mineralogical and chemical compositions: a case study from size-fractional sediments of the Huanghe (Yellow River) and Changjiang (Yangtze River). Geol. J. 50, 414–433.